Petroleum generation kinetics: Single versus multiple heating-ramp open-system pyrolysis

Kenneth E. Peters, Alan K. Burnham, and Clifford C. Walters

ABSTRACT

Some recent publications promote one-run, open-system pyrolysis experiments using a single heating rate (ramp) and fixed frequency factor to determine the petroleum generation kinetics of source-rock samples because, compared to multiple-ramp experiments, the method is faster, less expensive, and presumably yields similar results. Some one-ramp pyrolysis experiments yield kinetic results similar to those from multiple-ramp experiments. However, our data for 52 worldwide source rocks containing types I, II, IIS, II/III, and III kerogen illustrate that one-ramp kinetics introduce the potential for significant error that can be avoided by using high-quality kinetic measurements and multiple-ramp experiments in which the frequency factor is optimized by the kinetic software rather than fixed at some universal value. The data show that kinetic modeling based on a discrete activation energy distribution and three different pyrolysis temperature ramps closely approximates that determined from additional runs, provided the three ramps span an appropriate range of heating rates. For some source rocks containing well-preserved kerogen and having narrow activation energy distributions, both single- and multiple-ramp discrete models are insufficient, and nucleation-growth models are necessary. Instrument design, thermocouple size or orientation, and sample weight likely influence the acceptable upper limit of pyrolysis heating rate. Caution is needed for ramps of 30–50°C/min, which can cause temperature errors due to impaired heat transfer between the oven, sample, and thermocouple. Compound volatility may inhibit pyrolyzate yield at the lowest heating rates, depending on the effectiveness of the gas sweep. We recommend at least three pyrolysis ramps that span at least a 20-fold variation of comparatively lower rates, such as 1, 5, and 25°C/min. The product of heating rate and

Manuscript received May 9, 2014; provisional acceptance September 5, 2014; revised manuscript received October 6, 2014; final acceptance November 14, 2014.
DOI: 10.1306/11141414080

AUTHORS

KENNETH E. PETERS ~ *Schlumberger Information Solutions, 18 Manzanita Place, Mill Valley, California 94941; Department of Geological and Environmental Sciences, Stanford University, 450 Serra Mall, Stanford, California 94305; kpeters2@slb.com*

Kenneth E. Peters is science advisor for Schlumberger, having 36 years in industry, government, and academia. He is principal author of *The Biomarker Guide* (2005), author or co-author of more than 130 peer-reviewed scientific papers, honorary teaching fellow at the University of Aberdeen, a NExT instructor, fellow in the Geochemical Society, Charles Taylor fellow, and a consulting professor at Stanford University, where he co-leads the Basin and Petroleum System Modeling Industrial Affiliates Program (bpsm.stanford.edu). He is an associate editor for *AAPG Bulletin* and *Organic Geochemistry*. He is principal editor of the 2012 AAPG Hedberg Series 4 volume, *Basin Modeling: New Horizons in Research and Applications*; editor for the 2009 AAPG compact disk, *Getting Started in Basin and Petroleum System Modeling*; and co-editor for SEPM Special Publication 103, *Analyzing the Thermal History of Sedimentary Basins: Methods and Case Studies*. He was chair of the 1998 Gordon Research Conference on Organic Geochemistry, Chair of the AAPG Research Committee (2007–2010), and AAPG Distinguished Lecturer (2009–2010). In 2009, he received the Alfred E. Treibs Award presented by the Geochemical Society to scientists who have had a major impact on the field of organic geochemistry through long-standing contributions. In 2013, he received the AAPG Honorary Member Award, bestowed on those who have distinguished themselves by service and devotion to petroleum geology and the association. He twice received the Schlumberger Henri Doll Prize for Innovation (2009 and 2013). He has B.A. and M.A. degrees in geology from the University of California at Santa Barbara and a Ph.D. in geochemistry from the University of California at Los Angeles.

ALAN K. BURNHAM ~ *American Shale Oil, LLC, 4221 Findlay Way, Livermore, California 94550; aburnham@amso.net; akburnham@comcast.net*

Alan K. Burnham is chief technology officer of American Shale Oil, LLC (www.amso.net), which is conducting a pilot project on an oil shale research, development, and demonstration lease in Colorado from the US Bureau of Mines. He is also an adjunct professor of chemical engineering at the University of Utah and a consultant for GeoIsoChem Corporation. Previously, he spent more than 30 years at Lawrence Livermore National Laboratory (LLNL), working on and managing a variety of projects in energy research and national security. He developed kinetic models of vitrinite reflectance and petroleum formation that are widely used in basin modeling and is the co-developer of the Kinetics05 software (and predecessors) for chemical kinetic analysis. He has been a member of numerous professional societies, including the ACS, SPE, NATAS, EAOG, and AAPG. He is currently the chair of the oil shale subcommittee of the Energy Minerals Division of the AAPG, and he was previously an officer of the Geochemistry Division of the ACS. He is currently on the editorial board of *Thermochimica Acta* and was previously on the editorial board of *Energy and Fuels*. He received a Federal Laboratory Consortium Award for Technology Transfer in 1990 and was a 10th Anniversary Fellow at Norsk Hydro and the University of Bergen in 1992. He is author or co-author of 110 journal articles, 85 conference proceedings and book chapters, 54 publicly available LLNL technical reports, and 10 patents. He received a B.S. degree in chemistry from Iowa State University and a Ph.D. in physical chemistry from the University of Illinois at Champaign-Urbana.

CLIFFORD C. WALTERS ~ *ExxonMobil Research and Engineering Co., 1545 Route 22 East, Annandale, Clinton, New Jersey 08801-0998; clifford.c.walters@exxonmobil.com*

Clifford C. Walters completed his undergraduate studies at Boston University and in 1981 received a Ph.D. from the University of Maryland, where he conducted

sample size should not exceed ~100 mg °C/min. Our results do not address the more fundamental questions of whether kinetic models based on multiple-ramp open-system pyrolysis are mechanistically appropriate for use in basin simulators or whether petroleum migration through the kerogen network, rather than cracking of organic matter, represents the rate-limiting step in expulsion.

INTRODUCTION

Computerized basin and petroleum system modeling (BPSM) is a quantitative extension of early concepts of the dynamic petroleum system (e.g., Magoon and Dow, 1994; Hantschel and Kauerauf, 2009; Peters et al., 2012). Since its inception about 30 yr ago (Welte and Yükler, 1981; Espitalié et al., 1988; Welte et al., 1997), BPSM has grown from a simple tool to predict regional thermal maturity of subsurface petroleum source rocks to a more comprehensive and widely accepted component in exploration programs for both conventional and unconventional resources. Unconventional reservoirs represent those combinations of reservoir permeability and fluid viscosity that require stimulation, such as hydraulic fracturing, for production of oil or gas. Highly permeable sandstones that contain viscous heavy oil in intergranular porosity and tight shales that contain abundant hydrocarbon gas trapped in residual kerogen are examples of unconventional resources. Kerogen is the insoluble organic matter in sedimentary rock.

Current BPSM software incorporates a growing arsenal of algorithms that can be used to quantify relationships among the elements and processes of the petroleum system, including source, reservoir, seal, overburden, trap formation, and the generation–migration–accumulation of petroleum. For example, some recent developments in BPSM include modules to predict the extent of biodegradation or thermochemical sulfate reduction in conventional reservoirs or the composition of residual petroleum in unconventional reservoirs (Peters et al., 2013). Nevertheless, kinetic calculations remain as the core technology upon which these additional computations are based.

Understanding kinetic controls on the transformation of organic matter to petroleum is important because they are required to compute petroleum yields and generation rates in BPSM. Early work summarized by Tissot and Espitalié (1975) showed that the laboratory maturation of organic matter in source-rock samples can be described by a series of independent first-order reactions and the corresponding kinetic parameters. Such kinetic parameters were used in some of the earliest BPSM simulations (e.g., Sweeney et al., 1987; Espitalié et al., 1988; Issler and Snowdon, 1990; Ungerer, 1990).

The purpose of this paper is to compare the reliability of various combinations of open-system pyrolysis heating rates to determine the kinetics of petroleum generation in source rocks. Most industry and academic laboratories use multiple heating-ramp experiments to measure source-rock kinetics. In an attempt to reduce expense and turnaround time, Waples et al. (2002, 2010; Waples and Nowaczewski, 2013) introduced single-ramp kinetics, which they deem to be as reliable as multiple-ramp kinetics. They conclude that the single-ramp method decreases analysis time by a factor of ~20 and can be applied to archived Rock-Eval, Source Rock Analyzer, or other pyrolysis data. According to Waples and co-workers, the key to single-ramp kinetics is to use a fixed pre-exponential or frequency factor ($A = 1 \times 10^{14}$ or 2×10^{14} sec^{-1}), which constrains non-unique activation energy (E_a, kcal/mol) distributions to a single geologically reasonable result. The frequency factor is the pre-exponential constant in the Arrhenius equation (equation 1), which depends on vibrational frequency of the chemical bonds being broken, among other factors.

$$k = Ae^{-E_a/RT} \quad (1)$$

The Arrhenius equation relates the rate constant of a chemical reaction (k) to the temperature (T, Kelvin), where E_a is the activation energy and R is the universal gas constant. For first-order reactions, A has units of sec^{-1}. Increased temperature increases reaction rate. The universal frequency factor proposed by Waples and Nowaczewski (2013) is based on the average value for 259 source-rock determinations from the literature in which both E_a and A were optimized.

Assessing the validity of the method of Waples and co-workers (Waples et al., 2002, 2010; Waples and Nowaczewski, 2013) using a pre-assigned universal frequency factor involves addressing three questions.

1. Are there real differences in the frequency factors for different kerogens?
2. Are the differences large enough to have a significant impact on extrapolation to geological conditions?
3. What experimental conditions are required to answer questions 1 and 2?

We assume that the thermal alteration of organic matter in source rocks can be described by a set of sequential, independent, and parallel first-order reactions following the Arrhenius equation (e.g., Ungerer and Pelet, 1987). The assumption of independent parallel first-order reactions may be oversimplified (Stainforth, 2009), because petroleum generation involves complex radical

field and laboratory research on metasediments from Isua, Greenland, the oldest sedimentary rocks on Earth. Joining Gulf Research and Development in 1982, he implemented a program in biological marker compounds. In 1984, he moved to Sun Exploration and Production Company, where he was responsible for establishing biomarker geochemistry and thermal modeling as routine exploration tools. Mobil's Dallas Research Lab hired him in 1988, where he became supervisor of the Geochemical Laboratories. He is now with ExxonMobil Corporate Strategic Research, where he conducts research on modeling of oil generation and reservoir transformations, geomicrobiology, and solid bitumen formation. In recent years, he has led research programs in shale gas and polar biomarkers and has promoted the application of new analytical methods involving ultra-high-resolution mass spectrometry and helium ion microscopy. He has published numerous papers related to petroleum geochemistry and has co-authored a major treatise, *The Biomarker Guide*. He currently is an associate editor for *Organic Geochemistry* and serves on the executive committee for the Organic Geochemistry Division of the Geochemical Society.

ACKNOWLEDGEMENTS

We thank Schlumberger reviewers Robert Kleinberg, Drew Pomerantz, Bjorn Wygrala, Susan Duffield, and AAPG reviewers Robert Braun, Rolando di Primio, Ronald Hill, Dan Jarvie, and Barry Katz for their useful comments. Note that the authors and the authors' companies do not warrant or guarantee the success of well operations incorporating methods suggested herein.

cracking reactions, including initiation, propagation, and termination steps in which free radicals play a key role, as well as acid thermolysis and carbonium ion reactions with α-olefins (Kissin, 1987). Flynn and Florin (1985) provide a comprehensive review of thermal degradation mechanisms for macromolecular materials and discuss practical aspects of kinetic modeling based on nonisothermal data. Walters et al. (2007) derived a mechanistic model of kerogen pyrolysis from a detailed structure of kerogen and applied it to laboratory and geological conditions.

Several publications address optimizing kinetic parameters from open-system programmed pyrolysis. Braun and Burnham (1987) showed that fitting to a single heating rate does not yield reliable kinetic results for source rocks when both E_a and A were optimized. Model fitting based on single-ramp kinetics was deemed unacceptable by Vyazovkin and Wight (1999), and it is specifically discouraged by the Kinetics Committee of the International Confederation for Thermal Analysis and Calorimetry (Vyazovkin et al., 2011).

Sundararaman et al. (1992) also showed that one pyrolysis heating ramp does not give a reliable distribution of discrete activation energies for kerogens, although, unlike the approach of Waples et al. (2002, 2010), the frequency factor was optimized rather than fixed. Similar to later work by Dieckmann (2005), Sundararaman and co-workers showed that the assumption of a single optimized frequency factor for all possible activation energies associated with a discrete distribution can lead to erroneous results, particularly for type III kerogens, which show broad activation energy distributions. They concluded that to obtain reliable results, the pyrolysis experiments must be performed at two or three widely differing heating rates. Robust computed estimates of the discrete activation energy distributions of kerogens based on these pyrolysis experiments are best accomplished using an energy spacing of 1 kcal/mol or less. Sundararaman et al. (1992) also conducted an experiment that mixed liptinite and vitrinite having significantly different frequency factors. The assumption of a single optimized frequency factor for all possible activation energies in the discrete distribution for the mixture resulted in an incorrect activation energy distribution.

Various laboratory methods other than open-system programmed pyrolysis have been proposed to predict the thermal behavior of organic matter during burial maturation. These methods include closed-system isothermal pyrolysis, such as hydrous pyrolysis (e.g., Lewan et al., 1979; Lewan and Ruble, 2002), microscale sealed vessel pyrolysis (e.g., Horsfield et al., 1989), or gold tube reactors (e.g., Behar et al., 1992). Debate continues as to the reliability of kinetics determined using open- versus closed-system pyrolysis (e.g., Schenk and Horsfield, 1993; Ritter et al., 1995; Barth et al., 1996; Lewan and Ruble, 2002). This paper does not address that issue, but instead focuses on open-system pyrolysis and distributed activation energy models for organic matter decomposition to petroleum, because most source-rock kinetic parameters are obtained using these methods. Measured and predicted petroleum generation rate curves from open-system pyrolysis experiments are similar to those from natural maturation series, suggesting that laboratory experiments can be used to reliably predict maturation over geologic time (e.g., Schenk and Horsfield, 1998). Kinetic predictions can be tested against natural data using BPSM, as exemplified in Kuhn et al. (2012, their figure 9). In addition, some authors consider primary migration of petroleum through kerogen in the source rock, rather than cracking of kerogen, is the rate-limiting step in petroleum expulsion (e.g., Stainforth, 2009). Although this may apply, most assessments of expulsion timing again are based on input from open-system pyrolysis, which is the focus of this paper.

For all methods, the ideal sample to determine the rate of thermal decomposition of organic matter to petroleum consists of organic-rich, unweathered source rock that has undergone diagenesis but has not yet generated appreciable amounts of petroleum (vitrinite reflectance equivalent ~0.3%–0.5%). However, caution must be applied for immature oxygen-rich kerogen, which may be prone to cross-linking reactions that are atypical of natural maturation (Burnham et al., 1995; Reynolds et al., 1995; Jarvie and Lundell, 2001). It is also critical to assess whether the organofacies in the sample is representative of the source rock, because the rate of thermal

decomposition of organic matter to petroleum based on laboratory experiments differs for different source rocks (Tegelaar and Noble, 1994).

When samples of thermally immature source rock are unavailable, it is common practice in BPSM to use default kinetic parameters for other source rocks deemed to contain organic matter similar to that in the study area based on either kerogen type (e.g., Waples et al., 1992) or depositional environment and stratigraphic age (e.g., Pepper and Corvi, 1995). However, kerogen type as defined by the Rock-Eval pyrolysis hydrogen index is not systematically linked to kinetic response, and it is not recommended to infer kerogen type or kinetics based on depositional environment of the source rock (Peters et al., 2006a). As a consequence, selected default kinetics obtained by analysis of a source rock from one basin may not apply to the source rock in another. For example, Peters et al. (2006a, their figure 4) completed kinetic analyses of 29 worldwide source-rock samples containing mainly type II kerogen using the same pyrolysis system employed in the present study. By assuming a heating rate of 1°C/m.y., they showed a range of 30°C in the calculated temperature at 50% transformation ratio (TR) among the samples. Three examples of common default kinetic models for type II kerogen (Pepper and Corvi, 1995; Behar et al., 1997; Dieckmann et al., 2000) also showed significant variations in the calculated temperature at 50% TR. For this reason, default kinetics should only be used when suitable samples from the study area are unavailable for direct measurement of kinetic response. In such cases, the influence of different default kinetic models can be used in sensitivity tests that compare their influence relative to other variables on simulation output. In this paper, we use a typical geologic heating rate of 3°C/m.y. to compare temperatures achieved at 10%, 50%, and 90% TR for source-rock samples having different kinetic parameters. The TR expresses the extent of conversion of the original kerogen generative potential to petroleum on a scale from 0% to 100% (Tissot and Welte, 1984).

Multiple sets of activation energy distributions and frequency factors for the Arrhenius relationship can predict the laboratory pyrolysis response for any source rock to similar levels of accuracy. These non-unique E_a distributions and frequency factors correlate in a form described as the compensation effect, which can be shown on a plot of log A versus E_a relative to corresponding reference values (Figures 1, 2), derived by taking the logarithm of the rearranged Arrhenius equation 1:

$$\log A - \log A_{ref} = (E_a - E_{ref})/2.303RT \qquad (2)$$

Figure 1 shows that errors in the derivation of E_a and A determined by laboratory experiments can result in poor extrapolations of temperatures for petroleum generation under geologic conditions. The ellipses represent the loci of solutions with equal residual errors at varying levels of residual error for kinetic parameter optimization and the resulting range of geological temperature predictions. As a simple rule, along the major axes of the ellipses, variation of a factor of 2 in the frequency factor is approximately compensated by a 1 kcal/mol shift in

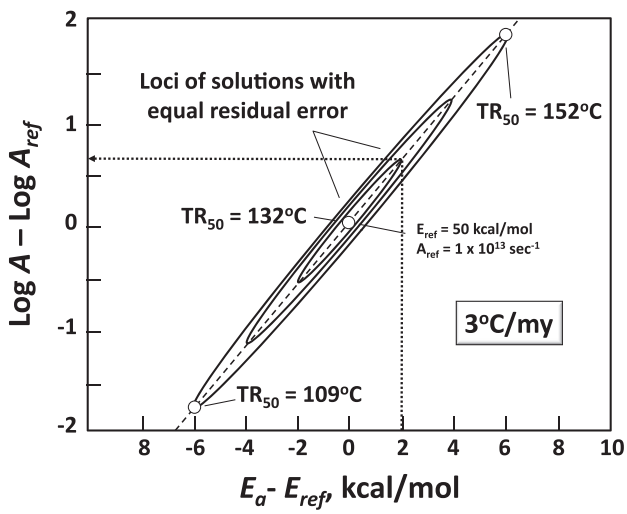

Figure 1. Ellipsoidal loci of geologic temperature predictions having activation energy (E_a, kcal/mol) or frequency factor (A, sec^{-1}) error relative to a reference value (E_{ref} or A_{ref}) display an Arrhenius compensation effect. The compensation effect results in multiple combinations of E_a and A that satisfy the laboratory reaction rate, but predicted temperatures deviate appreciably at geologic heating rates. TR_{50} is the calculated geologic temperature at 50% transformation ratio (TR), assuming a 3°C/m.y. heating rate, which differs depending on error relative to the reference value. Doubling of A is compensated by ~1 kcal/mol shift in the average E_a. The dotted line shows an example in which an E_a error of 2 kcal/mol corresponds to roughly a four-fold increase in A, that is, $\log(4) = 0.6$. Modified from Burnham (1992) and used with permission of AAPG.

the activation energy and a 3°C shift in the geological temperature prediction. For the purpose of this paper, an order of magnitude error in the frequency factor makes about a 10°C error in the extrapolation to geological heating rates.

Lakshmanan et al. (1991) also concluded that multiple kinetic solutions behave differently when extrapolated to geological heating rates. Unfortunately, like Ungerer and Pelet (1987), these authors set the reaction channels at 2 kcal/mol spacing, which typically yields poor optimizations. Large energy spacings can result in multiple local minima (e.g., Sundararaman et al., 1992, their figure 6). Reducing the energy spacing from 2 to 1 kcal/mol yields a single minimum, except for certain lacustrine kerogens having very narrow E_a distributions (Braun et al., 1991b). In our study, the reaction channels were set at 1 kcal/mol, as recommended by Braun et al. (1991b).

Once appropriate samples have been acquired, three criteria must be met to extrapolate Arrhenius kinetic parameters from experimental to geologic time scales (Braun et al., 1991b): (1) the experimental data must be accurate, (2) the appropriate reaction model must be used to evaluate the data, and (3) any changes in reaction mechanisms from experimental to geologic rates must not deviate from the Arrhenius law. The following discussion describes how these programmed heating experiments satisfy criteria 1 and 2. However, criterion 3 can only be handled empirically and is not addressed in this paper.

SAMPLES

Twenty-nine of the 52 well-characterized source-rock samples in this study were previously described by Peters et al. (2006a; Table 1). The remaining 23 samples were part of the original dataset but were not included in that publication. These cleaned drill cuttings, core, or outcrop samples are from worldwide collection localities, span the range of kerogen composition (from type I, II, IIS, II/III, and III, as defined by Rock-Eval pyrolysis hydrogen index, sulfur content, and organic petrography), and are immature to slightly mature with respect to oil generation (~0.4%–0.7% equivalent vitrinite reflectance). For most of the samples, ~5–10 g of rock was ground to a fine powder (~150 mesh) in an agate mortar and pestle before the pyrolysis experiments. One sample containing type II kerogen was collected from an outcrop on Bellagio Road, north of Sunset Boulevard near the University of California, Los Angeles. The outcrop consists of middle to upper Miocene (Mohnian Stage) lower Modelo Formation, which is an equivalent of the Monterey Formation source rock. Approximately 25 g of the rock was processed to assure homogeneity for use as a procedural standard and check for reproducibility.

METHODS

Pyrolysis of the source-rock samples was completed using Pyromat II (Lab Instruments, Inc.) open-system micropyrolysis. For each rock sample, 3–10 mg aliquots were pyrolyzed at one or more of the following rates: 1, 3, 5, 10, 30, and 50°C/min. In general, larger samples were used for organic-lean, lower heating-rate experiments, and vice versa.

Opinions differ on whether source-rock kinetic measurements should be completed using whole rock, extracted rock, or isolated kerogen. We used whole rock in this study for several reasons. (1) Waples et al. (2010) suggest that the single-ramp method is amenable to archived Rock-Eval pyrograms, which are normally obtained using whole rock. To compare single and multiple ramp experiments in our paper, it was therefore necessary to use whole rock. (2) The range of frequency factors for the 259 source rocks used by Waples and Nowaczewski (2013) to establish their universal value of A is based mainly on published whole-rock kinetics. (3) Most thermally immature source rocks have low extractable bitumen content unless contaminated by migrated oil or oil-based drilling additives. For example, Rock-Eval production indices for most immature source rock are low ($PI = S1/[S1 + S2] \leq 0.02$; Peters and Cassa, 1994). For such samples that are uncontaminated by migrated oil or additives, S1 and S2 represent bitumen and kerogen, respectively. The S1 peak represents hydrocarbons that can be thermally distilled by pyrolysis at 300°C

Table 1. Discrete Activation Energy (E_a) Distribution Modeling (Kinetics05) Completed for 52 Worldwide Source-Rock Samples (Peters et al., 2006a) Containing Types I, II, IIS, II/III, or III Kerogen*

Sample	Formation	Age	Country	E_a Single–Multi (kcal/mol)	Log A Single–Multi	Temp. at 50% TR, Multi Run (°C)	Temp. at 50% TR, Single Run (°C)	Δ Temp. Multi–Single at 50% TR (°C)	Kerogen Type**
1	Old Red Sandstone	Devonian	Scotland	3.78	1.23	134.8	147.5	–12.7	I
2	Holy Cross Mountains	Devonian	Poland	–3.11	–0.97	202.2	189.4	12.8	II
3	Strathcylde Croup Lothian Shale	Mississippian	U.K.	–1.49	–0.40	158.2	153.5	4.6	I
4	Westphalian Cannel Coal	Pennsylvanian	U.K.	0.53	0.23	153.0	154.8	–1.8	III
5	Marl Slate	Permian	U.K.	0.66	0.23	139.2	141.4	–2.2	II
6	Kupferschiefer	Permian	Poland	0.83	0.24	137.9	140.6	–2.7	II
7	Besano Oil Shale–Meride Limestone	Triassic	Italy	0.25	0.24	138.0	138.5	–0.5	II/III
8	Botneheia Member	Triassic	Norway	0.52	0.20	152.7	154.5	–1.8	II
9	Jet Rock Bitumenous Shale	Jurassic	U.K.	–0.96	–0.23	154.0	150.2	3.8	II
10	Posidonian Shale	Jurassic	Netherlands	2.22	0.67	145.4	152.7	–7.3	I/II
11	Kimmeridge Clay	Jurassic	U.K.	–0.54	–0.11	146.0	143.7	2.3	II
12	Mirodekhinskaya	Riphean	Russia	3.78	1.21	137.6	149.9	–12.3	II
13	Domanic Shale	Devonian	Russia	3.69	1.18	138.5	151.0	–12.5	I
14	Aibolinskaya Sazymbaiskaya	Jurassic	Russia	1.89	0.66	156.5	163.7	–7.2	II
15	Bazhenov	Jurassic	Russia	4.31	1.39	136.6	151.5	–14.9	II
16	Maykop	Oligocene	Russia	2.93	1.00	141.5	150.7	–9.3	III
17	Etolonskiy	Miocene	Russia	2.61	0.79	148.7	156.8	–8.1	III
18	Lucaogou	Permian	China	–3.33	–0.99	164.4	153.6	10.8	I
19	Dameigou–Xiaomeigou	Jurassic	China	–1.65	–0.47	155.2	149.8	5.3	I
20	Guchengzi	Eocene	China	–0.21	0.04	151.0	150.3	0.6	I
21	Youganwo	Eocene	China	–0.64	–0.15	149.8	147.6	2.2	I
22	Dingo Claystone	Jurassic	Australia	–0.30	–0.10	156.2	154.9	1.3	II/III
23	Toolebuc	Cretaceous	Australia	0.01	0.07	140.5	139.9	0.6	II
24	Huqf Group	Precambrian	Oman	2.32	0.68	145.2	153.8	–8.6	II
25	Rhazziane Azzel	Ordovician	Algeria	1.46	0.54	148.5	153.6	–5.1	II
26	Dadas	Silurian	Turkey	1.63	0.53	145.1	150.3	–5.2	II
27	Diyab	Jurassic	U.A.E.	–0.86	–0.17	158.8	156.2	2.5	II
28	Madbi	Jurassic	Yemen	0.25	0.09	151.3	152.1	–0.8	II
29	Shilaif	Cretaceous	U.A.E.	3.04	0.96	138.7	149.4	–10.7	IIS
30	Natih	Cretaceous	Oman	0.25	0.05	140.2	141.5	–1.3	IIS
31	Duwi	Cretaceous	Egypt	0.43	0.20	143.0	144.3	–1.2	II
32	Thebes	Eocene	Egypt	1.47	0.53	137.3	142.2	–4.9	IIS
33	Stanleyville	Jurassic	Zaire	–2.02	–0.62	156.9	150.6	6.3	I
34	Uarandab	Jurassic	Ethiopia	0.71	0.24	141.2	143.5	–2.3	II
35	Abu Gabra	Cretaceous	Sudan	–2.16	–0.66	161.8	155.3	6.5	I
36	Pre-salt	Cretaceous	Gabon	–3.02	–0.94	165.1	156.3	8.9	I

(*continued*)

Table 1. Continued

Sample	Formation	Age	Country	E_a Single–Multi (kcal/mol)	Log A Single–Multi	Temp. at 50% TR, Multi Run (°C)	Temp. at 50% TR, Single Run (°C)	Δ Temp. Multi–Single at 50% TR (°C)	Kerogen Type**
37	Bakken	Devonian	U.S.A.	1.46	0.46	142.3	147.1	–4.7	II
38	Ohio Shale	Devonian	U.S.A.	0.98	0.42	150.5	154.3	–3.7	II
39	Mowry	Cretaceous	U.S.A.	3.08	0.91	137.7	148.3	–10.6	II/III
40	Greenhorn	Cretaceous	U.S.A.	3.83	1.21	133.4	145.7	–12.3	II
41	Niobrara	Cretaceous	U.S.A.	–0.73	–0.18	158.1	155.9	2.2	II
42	Green River	Eocene	U.S.A.	2.27	0.69	142.1	150.1	–8.0	I
43	Monterey	Miocene	U.S.A.	–1.11	–0.22	130.9	127.8	3.1	IIS
44	Duvernay	Devonian	Canada	1.02	0.39	152.2	155.7	–3.5	II
45	Exshaw	Mississippian	Canada	1.91	0.66	144.2	151.1	–6.9	II
46	Doig	Mississippian	Canada	–1.88	–0.48	161.3	155.5	5.8	II
47	Fernie (Nordegg Member)	Jurassic	Canada	–0.48	–0.06	149.9	148.1	1.8	II
48	Second White Speckled Shale	Cretaceous	Canada	2.59	0.91	139.5	149.1	–9.6	II
49	Polier Mudstone	Cretaceous	Cuba	0.11	0.13	152.0	152.1	–0.1	II
50	Sabanilla Mudstone	Cretaceous	Cuba	2.96	0.89	139.3	149.3	–10.0	II
51	Napo	Cretaceous	Ecuador	3.43	1.06	128.2	140.7	–12.5	IIS
52	La Luna	Cretaceous	Colombia	3.51	1.15	133.7	145.5	–11.9	II

*Multi data are based on analysis of 1, 3, 5, 10, 30, and 50°C/min multiple-ramp Pyromat II pyrolysis experiments in which the frequency factor (A) was optimized rather than fixed at 1×10^{14} sec^{-1} (as for the single data). Calculated temperatures assume a 3°C/m.y. geologic heating rate. Columns 5 and 6 are plotted in Figure 2, and columns 7 and 8 are plotted in Figure 3. TR = transformation ratio.

**Type I, II, II/III, and III kerogens have hydrogen indices >600, 300–600, 200–300, and 50–200 mg hydrocarbon/g total organic carbon, and type IIS kerogens show high sulfur (i.e., 8–14 wt.%) or atomic sulfur/carbon ≥ 0.04 (Peters and Cassa, 1994).

(mg hydrocarbon/g rock), whereas S2 represents hydrocarbons cracked from kerogen by pyrolysis at higher temperatures. Tegelaar and Noble (1994) and Reynolds and Burnham (1995) showed these types of whole-rock samples yield kinetic parameters similar to the isolated kerogen. (4) Although it is well known that bitumen in some immature source-rock samples may contribute to the pyrolysis peak generated by the cracking of kerogen (e.g., Clementz, 1979; Peters, 1986; Jarvie, 1991), we maintain that whole rock rather than extracted rock or isolated kerogen provides a better indication of the kinetic response of the bulk organic matter (kerogen plus bitumen) during burial maturation.

Continuous temperatures were measured during each pyrolysis experiment using a calibrated thermocouple that was in direct contact with the sample in the furnace. Products were transferred to a flame ionization detector by helium flow at 50 ml/min. The resulting pyrolyzate peaks for decomposition of the kerogen were processed using Kinetics05 software, which derives chemical kinetic parameters (Burnham and Braun, 1999). The model parameters were determined by iterative linear–nonlinear regression, in which energy weighting factors are determined by constrained linear regression for a given frequency factor and the logarithm of the frequency factor is varied under Levenberg–Marquardt nonlinear regression (Levenberg, 1944) until the root mean squared deviation between observed and calculated generation rates of pyrolyzate yield reach a minimum. Only the weighting factors are optimized for a fixed A.

Depending on kerogen structure, the thermal reactivity of kerogen can be described by a reactivity distribution of E_a values or an autocatalytic reaction profile of time versus cumulative conversion.

Energy spacing through the E_a distribution is important. In these kinetic calculations, the frequency factor is used as an optimizing variable. Pyrolyzate peaks in this study were fit (optimized) using the discrete activation energy distribution method in Kinetics05 software with an energy spacing of 1 kcal/mol and one optimized frequency factor (Burnham et al., 1987). We used the discrete reactivity model rather than a Gaussian or other model because E_a distributions for source rocks can be broad and asymmetric. The extent of kerogen conversion was calculated by summing the first-order contributions over the entire distribution of energies. Some samples were also analyzed using the nucleation-growth (autocatalytic) model, which is recommended for samples having narrow E_a distributions (Burnham et al., 1996). These kerogens have unusual reaction characteristics under isothermal conditions; the reaction rate gradually increases with time at constant temperature before reaching a peak and then decreasing. This is unlike most kerogens, in which the initial peak reaction rate continuously decreases with time. These unusual reaction characteristics are shared with linear polymers, for which multiple bond-breaking events are needed to form a volatile product. Nucleation growth has characteristics similar to a sequential reaction (Burnham et al., 1996) and to a random-scission model, which is also used for linear polymer decomposition (Sanchez-Jimenez et al., 2010).

The single-ramp experiments were processed by the Kinetics05 software using a fixed frequency factor of 1×10^{14} sec^{-1} as recommended by Waples et al. (2002, 2010), although Waples and Nowaczewski (2013) recommend a frequency factor of 2×10^{14} sec^{-1}. For all other experiments using two or more heating rates, the frequency factor was optimized by Kinetics05. For all samples, the correlation between true T_{max} and the log of the heating rate was linear with a high correlation coefficient ($r^2 > 0.99$), as would be expected from the Ozawa–Flynn–Wall equation if T_{max} occurs at the same level of conversion at each heating rate (Ozawa, 1965; Flynn and Wall, 1966; Vyazovkin et al., 2011). T_{max} is the sample temperature corresponding to the maximum yield of pyrolyzate during each heating experiment.

RESULTS AND DISCUSSION

The following results show that kinetic parameters for petroleum generation from source-rock organic matter can be measured with sufficient precision in the laboratory to invalidate the use of a fixed, universal value of the frequency factor. Furthermore, we show that multiple-ramp pyrolysis experiments are consistently more reliable than single-ramp experiments for determining kinetic parameters.

Precision of Experimental Data

Useful kinetic parameters require acquisition of good data (Vyazovkin et al., 2014). Three types of errors must be addressed (Appendix): (1) a constant shift in all measurement temperatures, (2) a temperature error that varies systematically with temperature or heating rate, and (3) random error. First, reproducible systematic error in temperature can occur for several reasons, such as an improperly calibrated thermocouple. The second error type depends on heating rate, such as a thermal transient that becomes larger at faster heating rates. Various factors can cause random error, including slight variations in the spatial arrangement of the thermocouple and sample in different experiments. The standard deviation defines how many measurements are needed to have confidence that the average is within required tolerance. A systematic shift in temperature measurement (error type 1) is not as serious as an error that depends on heating rate (error type 2), as discussed by Burnham et al. (1987). According to Braun et al. (1991a), an error of 2°C at 50°C/min is the maximum that can be tolerated for reasonable extrapolations to geological time. Of these three error types, the reproducibility and thermal transient issues will be discussed in greater detail.

Bellagio Road Replicate Analyses

To test the variability of kinetic results for replicate analyses at a single pyrolysis heating rate, the Bellagio Road sample was analyzed 16 times (Table 2). Data from the 30°C/min pyrolyses were used for single-run models because that rate is most similar to Rock-Eval pyrolysis (25°C/min) (Note

Table 2. Statistics for 16 Single-Ramp (30°C/min) Pyromat II Pyrolysis Experiments for the Bellagio Road Sample Using a Fixed Frequency Factor ($A = 1 \times 10^{14}$ sec^{-1})*

	T_{max} (°C)	Average E_a (kcal/mole)	Temp. at 10% TR (°C)	Temp. at 50% TR (°C)	Temp. at 90% TR (°C)
Average	449.3	53.54	112.0	137.3	163.7
Minimum	447.8	52.97	105.2	135.8	160.4
Maximum	452.1	53.87	115.0	138.4	168.2
Std. dev.	1.3	0.28	2.3	0.8	2.2

*The data show that the best possible average activation energy for the sample determined by this method has a standard deviation of ±0.28 kcal/mol. Temperatures at 10%, 50%, and 90% transformation ratio (TR) were calculated assuming a geologic heating rate of 3°C/m.y.

that all quoted heating rates are nominal, but an exact heating rate is used for all calculations). The single-rate experiments using a fixed frequency factor as recommended by Waples et al. (2002, 2010; $A = 1 \times 10^{14}$ sec^{-1}) gave an average E_a of 53.54 ± 0.28 kcal/mol. Table 2 shows the calculated temperatures at 10%, 50%, and 90% TR, assuming a typical geologic heating rate of 3°C/m.y. The associated standard deviations represent the minimum uncertainty for geological extrapolation of single-ramp experiments using our Pyromat II. Replicate measurements on a set of samples by Burnham (1994), for which the frequency factor was optimized, give a standard deviation of ~1 kcal/mol with a compensating two-fold change in frequency factor, resulting in a standard deviation for geologic extrapolations of 3°C (1-2-3 rule), similar to our results and well within the range of geologic uncertainties.

The 52 samples examined in this work show a range of calculated frequency factors of about four orders of magnitude (~10^{12}–10^{16} sec^{-1}). These frequency factors are reproducible within experimental precision. Furthermore, Burnham (1994) saw a similar range in frequency factors for his samples. Using his 1-2-3 rule, he calculated that adoption of a fixed frequency factor of 1×10^{14} sec^{-1} could result in error for geologic extrapolations as large as 20°C. Thus, adoption of a single frequency factor of 1×10^{14} or 2×10^{14} sec^{-1} as recommend by Waples et al. (2002, 2010) and Waples and Nowaczewski (2013) is unwarranted. Our results are consistent with observations of solid-phase thermal decompositions, which show rates that can range up to six or seven orders in magnitude (Cordes, 1968). Note that although Waples and Nowaczewski (2013) list Rock-Eval as an appropriate tool for their single-ramp experiments, studies show that measured Rock-Eval temperatures can be tens of degrees lower than the actual temperature (Espitalié, 1986; Burnham et al., 1987). The temperature correction for Rock-Eval pyrolysis depends on the model of the instrument.

Global Comparison of Single- and Multiple-Run Kinetic Parameters

Comparison of kinetic parameters derived from single and up to six heating rates for the 52-sample suite shows that the impact of fixing the frequency factor is offset by adjustments of the average of the activation energy distribution in the Kinetics05 optimization (Figure 2). The figure illustrates the compensation effect as described by Burnham (1992), in which the difference in models using a fixed or optimized frequency factor is offset by the average E_a. The correlation holds for all kerogen types. However, when applying geologic heating rates to these models, the differences between them are magnified. Using a 3°C/m.y. heating rate, the single-run kinetic models yield temperatures at 50% conversion ranging from 17°C higher to 10°C lower than those derived from multiple heating-rate models with optimized frequency factors (Figure 3). These variations (i.e., vertical displacement from the dashed line in Figure 3) do not correlate with kerogen type, so our knowledge of the kerogen type cannot be used to adjust the single-run kinetics in a consistent manner. However, samples with higher generation temperatures at 50% TR (upper right in Figure 3) tend to have lower predicted temperatures (e.g., below the dashed line)

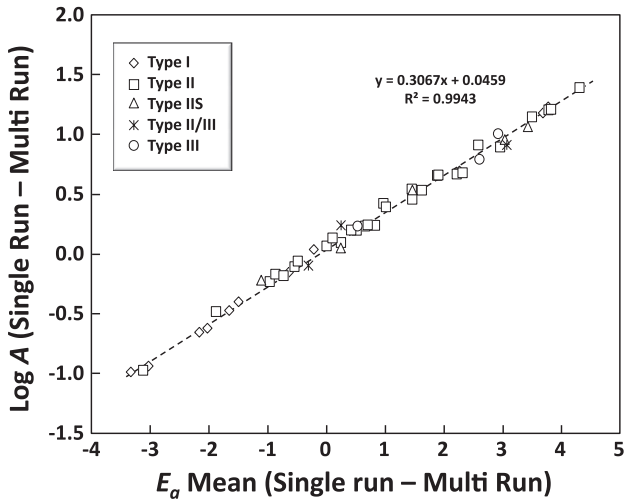

Figure 2. Comparison of kinetic results for 52 worldwide source-rock samples based on the difference between (1) 30°C/min pyrolysis using a single, fixed frequency factor ($A = 1 \times 10^{14}$ sec^{-1}) and (2) average of multiple pyrolyses (1, 3, 5, 10, 30, 50°C/min) using optimized A (Table 1, columns 5 and 6). The impact of fixing A in a single-ramp experiment is effectively offset by adjustments of the average E_a, regardless of kerogen type.

based on the single-ramp method, whereas samples with lower generation temperatures at 50% TR (lower left) tend to have higher predicted temperatures (e.g., above the dashed line).

Two Examples of the Effects of Single and Multiple Heating Rates

Two samples from the Kimmeridge Clay Formation and Monterey Shale (type II and IIS kerogen, respectively) were examined in detail (Table 3). Various combinations of experiments were used to optimize the kinetic parameters, including the frequency factor (Figure 4). Low heating-rate ratios (R_r = maximum divided by minimum rate) result in large variations in E_a and the corresponding frequency factor. For $R_r > 16$, the variability of E_a becomes relatively small. The dotted lines in the figure represent the temperature error in E_a (3σ) calculated from the standard deviation for the 16 Bellagio Road measurements. Therefore, $R_r > 16$ are desirable to minimize the error in E_a and A. Furthermore, statistical arguments indicate that multiple determinations, particularly at the lowest and highest heating rates, can improve the reliability of the answer, as shown in the Appendix.

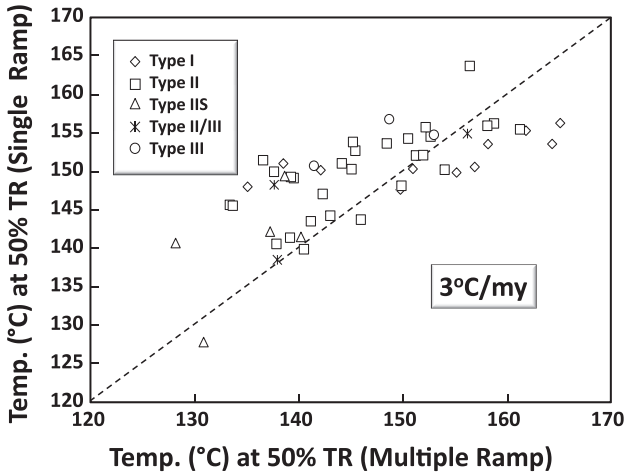

Figure 3. Assuming a 3°C/m.y. heating rate, the single-run kinetic models with a fixed frequency factor ($A = 1 \times 10^{14}$ sec^{-1}) yield calculated temperatures at 50% transformation ratio (TR) ranging from 17°C higher to 10°C lower than those from multiple kinetic models with optimized A (combinations of 1, 3, 5, 10, 30, and 50°C/min ramps; Table 1, columns 7 and 8). These variations do not correlate with kerogen type.

By plotting frequency factor and activation energy ($A - E_a$) pairs for $R_r > 16$, one can determine the probability that differences in the average A and E_a are real and not a measurement artifact. This compensation law comparison is shown in Figure 5. It is clear that the populations of the Kimmeridge Clay and Monterey Shale kinetic parameter determinations do not overlap, and A differs between the two samples by a factor of ~10.

The optimized frequency factor for the Kimmeridge Clay sample is 1.28×10^{14} sec^{-1}, similar to that recommended by Waples et al. (2002, 2010; 1×10^{14} sec^{-1}) for the single-run experiments, whereas the optimized frequency factor of 1.13×10^{13} sec^{-1} for the Monterey Shale sample is significantly lower. Figures 6 and 7 show calculated temperatures at 10%, 50%, and 90% TR for the Kimmeridge Clay and Monterey Shale samples. The plots are based on Kinetics05 optimized distributed reactivity models using various combinations of Pyromat II heating rates (1, 3, 5, 10, 30, and 50°C/min). The number of ramps in the figures (left) range from one to six and selected combinations of ramps are marked on the figure (Table 3). For example, the six-ramp experiment is labeled "1,3,5,10,30,50."

The range of predicted temperatures at 10%, 50%, and 90% TR using multiple ramps and optimized A

Table 3. Kinetics05 Temperatures Calculated at 10%, 50%, and 90% TR, Assuming a Geologic Heating Rate of 3°C/m.y. for Kimmeridge Clay and Monterey Shale Samples Classified by Pyrolysis Heating-Rate Ratio*

Sample	Heating-Rate Ratio (R_r)	Rate (°C/min)	Number of Ramps	E_a (kcal/mol)	A (sec^{-1})	Temp. at 10% TR (°C)	Temp. at 50% TR (°C)	Temp. at 90% TR (°C)
Kimmeridge Clay	1	1	1	53.71	1.00×10^{14}	125.7	145.2	164.4
	1	3	1	53.81	1.00×10^{14}	127.3	145.5	165.3
	1	5	1	53.59	1.00×10^{14}	125.2	144.6	164.4
	1	10	1	53.47	1.00×10^{14}	124.1	143.7	163.0
	1	30	1	53.65	1.00×10^{14}	126.4	145.0	163.3
	1	50	1	53.64	1.00×10^{14}	125.9	145.2	163.8
	2	5,10	2	60.42	1.49×10^{16}	142.5	164.9	186.0
	3	1,3	2	53.26	6.77×10^{13}	125.2	143.8	163.4
	3	10,30	2	49.30	4.83×10^{12}	112.7	129.5	147.5
	3.3	3,10	2	60.79	1.85×10^{16}	144.3	165.9	187.0
	3.3	3,5,10	3	60.78	1.78×10^{16}	143.8	165.7	186.8
	5	1,5	2	55.80	4.72×10^{14}	130.9	151.3	171.7
	5	10,50	2	49.74	6.75×10^{12}	113.7	131.1	149.2
	5	1,3,5	3	55.27	3.16×10^{14}	130.2	149.9	170.0
	5	10,30,50	3	49.69	6.41×10^{12}	113.8	130.9	148.9
	6	5,30	2	60.42	1.49×10^{16}	142.5	164.9	186.0
	6	5,10,30	3	52.54	4.76×10^{13}	122.4	141.1	160.0
	10	1,10	2	57.00	1.18×10^{15}	133.8	154.6	175.5
	10	3,30	2	54.86	2.18×10^{14}	130.0	148.8	168.4
	10	5,50	2	52.69	4.47×10^{13}	122.3	141.1	160.1
	10	1,3,10	3	57.13	1.25×10^{15}	134.8	155.2	175.6
	10	1,5,10	3	56.80	1.02×10^{15}	133.4	154.2	174.6
	10	3,5,30	3	53.52	8.87×10^{13}	125.7	144.6	164.0
	10	5,10,50	3	51.97	3.16×10^{13}	120.5	139.1	158.1
	10	5,30,50	3	52.63	4.91×10^{13}	122.9	141.6	160.3
	10	1,3,5,10	4	57.01	1.16×10^{15}	134.4	154.9	175.3
	10	3,5,10,30	4	54.54	1.88×10^{14}	128.3	147.6	167.2
	16.7	3,50	2	54.08	1.26×10^{14}	127.6	146.5	168.4
	16.7	3,5,50	3	53.52	8.87×10^{13}	125.7	144.6	164.0
	16.7	3,5,10,50	4	53.50	8.97×10^{13}	125.3	144.3	163.8
	16.7	3,5,10,30,50	5	53.48	8.63×10^{13}	125.3	144.2	163.5
	30	1,30	2	54.37	1.54×10^{14}	127.9	147.1	166.7
	30	1,3,30	3	54.45	1.63×10^{14}	128.4	147.4	167.0
	30	1,5,30	3	54.45	1.63×10^{14}	128.4	147.4	167.0
	30	1,10,30	3	54.65	1.98×10^{14}	128.2	147.8	167.6
	30	1,3,5,30	4	54.41	1.63×10^{14}	128.1	147.3	167.0
	30	1,5,10,30	4	54.63	1.95×10^{14}	128.1	147.7	167.6
	30	1,3,5,10,30	5	54.92	2.42×10^{14}	129.2	148.7	168.6
	50	1,3,5,10,30,50	6	54.01	1.28×10^{14}	126.8	146.0	165.1
	50	1,50	2	53.87	1.07×10^{14}	126.3	145.6	165.1
	50	1,3,50	3	53.91	1.12×10^{14}	126.9	145.9	165.4
	50	1,5,50	3	53.72	9.86×10^{13}	125.7	145.1	164.8
	50	1,10,50	3	53.91	1.17×10^{14}	126.1	145.5	165.2
	50	1,3,5,50	4	53.85	1.09×10^{14}	126.4	145.5	165.2

(*continued*)

Table 3. Continued

Sample	Heating-Rate Ratio (R_r)	Rate (°C/min)	Number of Ramps	E_a (kcal/mol)	A (sec^{-1})	Temp. at 10% TR (°C)	Temp. at 50% TR (°C)	Temp. at 90% TR (°C)
	50	1,5,10,50	4	53.90	1.15×10^{14}	125.9	145.4	165.2
	50	1,10,30,50	4	53.88	1.11×10^{14}	126.2	145.4	165.0
	50	1,3,5,10,50	5	53.98	1.20×10^{14}	126.9	146.0	165.6
	50	1,5,10,30,50	5	53.75	1.05×10^{14}	125.8	145.1	164.6
Monterey Shale	1	1	1	52.49	1.00×10^{14}	111.4	135.8	160.2
	1	3	1	52.36	1.00×10^{14}	109.6	135.3	160.1
	1	5	1	52.72	1.00×10^{14}	115.0	136.7	160.7
	1	10	1	52.39	1.00×10^{14}	107.5	136.0	161.6
	1	30	1	52.42	1.00×10^{14}	105.2	136.0	163.9
	1	50	1	52.61	1.00×10^{14}	106.5	136.9	165.7
	2	5,10	2	55.92	1.17×10^{15}	119.9	147.1	173.2
	3	1,3	2	50.29	1.81×10^{13}	105.9	129.3	153.0
	3	10,30	2	49.84	1.52×10^{13}	100.6	127.8	152.4
	3.3	3,10	2	50.53	2.29×10^{13}	104.7	130.1	154.5
	3.3	3,5,10	3	51.20	3.64×10^{13}	107.4	132.4	156.9
	5	1,5	2	48.61	4.86×10^{12}	101.3	123.9	147.1
	5	10,50	2	47.14	2.07×10^{12}	91.5	118.1	142.9
	5	1,3,5	3	48.78	5.67×10^{12}	101.6	124.4	147.7
	5	10,30,50	3	47.31	2.38×10^{12}	91.9	118.5	143.3
	6	5,30	2	52.38	8.70×10^{13}	109.7	136.5	161.8
	6	5,10,30	3	52.21	7.78×10^{13}	108.8	135.8	161.1
	10	1,10	2	50.53	2.27×10^{13}	105.2	130.0	154.2
	10	3,30	2	50.55	2.33×10^{13}	103.9	130.2	155.1
	10	5,50	2	50.18	7.88×10^{12}	99.7	125.7	151.1
	10	1,3,10	3	50.43	2.08×10^{13}	105.2	129.7	153.9
	10	1,5,10	3	50.25	1.78×10^{13}	104.9	129.2	153.3
	10	3,5,30	3	50.79	2.67×10^{13}	105.6	131.1	155.7
	10	5,10,50	3	48.89	6.81×10^{12}	98.8	124.7	149.7
	10	5,30,50	3	49.97	1.48×10^{13}	101.3	128.4	153.9
	10	1,3,5,10	4	50.21	1.74×10^{13}	104.9	129.1	153.2
	10	3,5,10,30	4	50.74	2.62×10^{13}	105.1	130.9	155.5
	16.7	3,50	2	48.54	5.07×10^{12}	97.4	123.5	149.0
	16.7	3,5,50	3	48.90	6.39×10^{12}	99.7	124.7	149.7
	16.7	3,5,10,50	4	48.88	6.53×10^{12}	99.4	124.6	149.5
	16.7	3,5,10,30,50	5	49.23	8.81×10^{12}	99.8	125.8	150.5
	30	1,30	2	50.41	2.06×10^{13}	104.0	129.6	154.4
	30	1,3,30	3	50.40	2.04×10^{13}	104.6	129.6	154.1
	30	1,5,30	3	50.57	2.23×10^{13}	105.3	130.3	154.9
	30	1,10,30	3	50.44	2.15×10^{13}	103.7	129.7	154.6
	30	1,3,5,30	4	50.47	2.10×10^{13}	105.2	129.9	154.2
	30	1,5,10,30	4	50.59	2.33×10^{13}	104.9	130.3	155.0
	30	1,3,5,10,30	5	50.60	2.32×10^{13}	105.2	130.3	155.0
	50	1,3,5,10,30,50	6	49.60	1.11×10^{13}	102.0	127.9	153.9
	50	1,50	2	49.00	6.92×10^{12}	99.4	125.0	150.1
	50	1,3,50	3	48.96	6.53×10^{12}	100.0	124.8	149.8

(*continued*)

Table 3. Continued

Sample	Heating-Rate Ratio (R_r)	Rate (°C/min)	Number of Ramps	E_a (kcal/mol)	A (sec^{-1})	Temp. at 10% TR (°C)	Temp. at 50% TR (°C)	Temp. at 90% TR (°C)
	50	1,5,50	3	49.03	6.89×10^{12}	100.4	125.2	149.9
	50	1,10,50	3	48.98	7.08×10^{12}	99.1	124.9	149.8
	50	1,3,5,50	4	48.96	6.50×10^{12}	100.6	125.0	149.6
	50	1,5,10,50	4	49.64	1.13×10^{13}	101.5	127.2	152.3
	50	1,10,30,50	4	49.31	9.32×10^{12}	99.6	126.0	151.2
	50	1,3,5,10,50	5	48.99	6.94×10^{12}	100.3	125.1	149.6
	50	1,5,10,30,50	5	50.59	2.33×10^{13}	104.9	130.3	155.0

*The single-ramp results consist of six pyrolysis experiments at 1, 3, 5, 10, 30, and 50°C/min, using a constant A factor (1×10^{14} sec^{-1}) as recommended by Waples et al. (2002, 2010). The two- through six-ramp results consist of all combinations of the six heating rates using an optimized frequency factor. The pyrolysis heating-rate ratio is calculated as the maximum divided by the minimum Pyromat II heating rates.

values (open symbols; Figures 6, 7) decreases with increasing (1) number of ramps and (2) heating-rate ratio, R_r. This decrease in predicted temperature is a statistical refinement due to replicate measurements and does not necessarily mean that additional intermediate heating rates are beneficial; replicates at the extreme heating rates are equally or more effective, as explained in the Appendix. More ramps and a broader range of ramp rates result in more precise temperature predictions. As discussed in detail below, the predicted temperatures for the Kimmeridge Clay at 10%, 50%, and 90% TR based on the six-ramp experiment (open symbols labeled "1,3,5,10,30,50") agree with those determined by the single-ramp, fixed A method of Waples et al. (2002, 2010) and Waples and Nowaczewski (2013) (i.e., solid symbols in

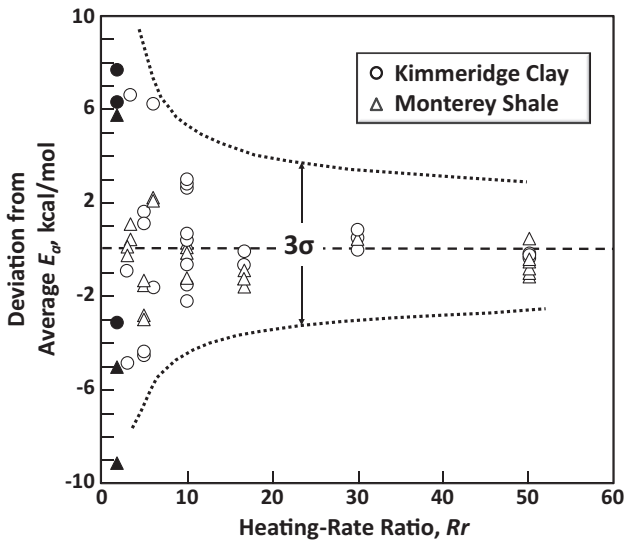

Figure 4. Deviation from average activation energy (E_a) versus heating-rate ratio (R_r = maximum divided by minimum rate) for samples from the Kimmeridge Clay and Monterey Shale (type II and IIS kerogen, respectively). Optimized kinetic parameters were calculated from one (solid symbols) or combinations of two to six heating-rate experiments (open symbols) in the range of 1, 3, 5, 10, 30, and 50°C/min. When R_r is low, the variability of E_a (and the corresponding frequency factor, A) is large. For heating-rate ratios $R_r > 16$, the variability of E_a becomes relatively small. Dotted curves represent the temperature error (3σ) in E_a calculated from the standard deviation for the 16 Bellagio Road measurements as a function of R_r (Table 2).

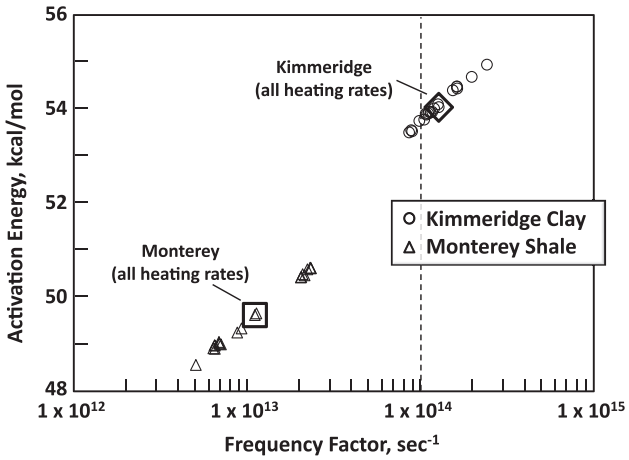

Figure 5. Plot of optimized frequency factor–activation energy ($A - E_a$) pairs for heating-rate ratios, $R_r > 16$ (Figure 4) shows that differences in the average A and E_a are real and not a measurement artifact. The Kimmeridge Clay and Monterey Shale kinetic parameters do not overlap, and the average frequency factor for the two samples based on all combinations of two to six heating rates (1, 3, 5, 10, 30, and 50°C/min; Table 3) differs by a factor of ~10. The dashed vertical line is the universal A from Waples et al. (2002, 2010).

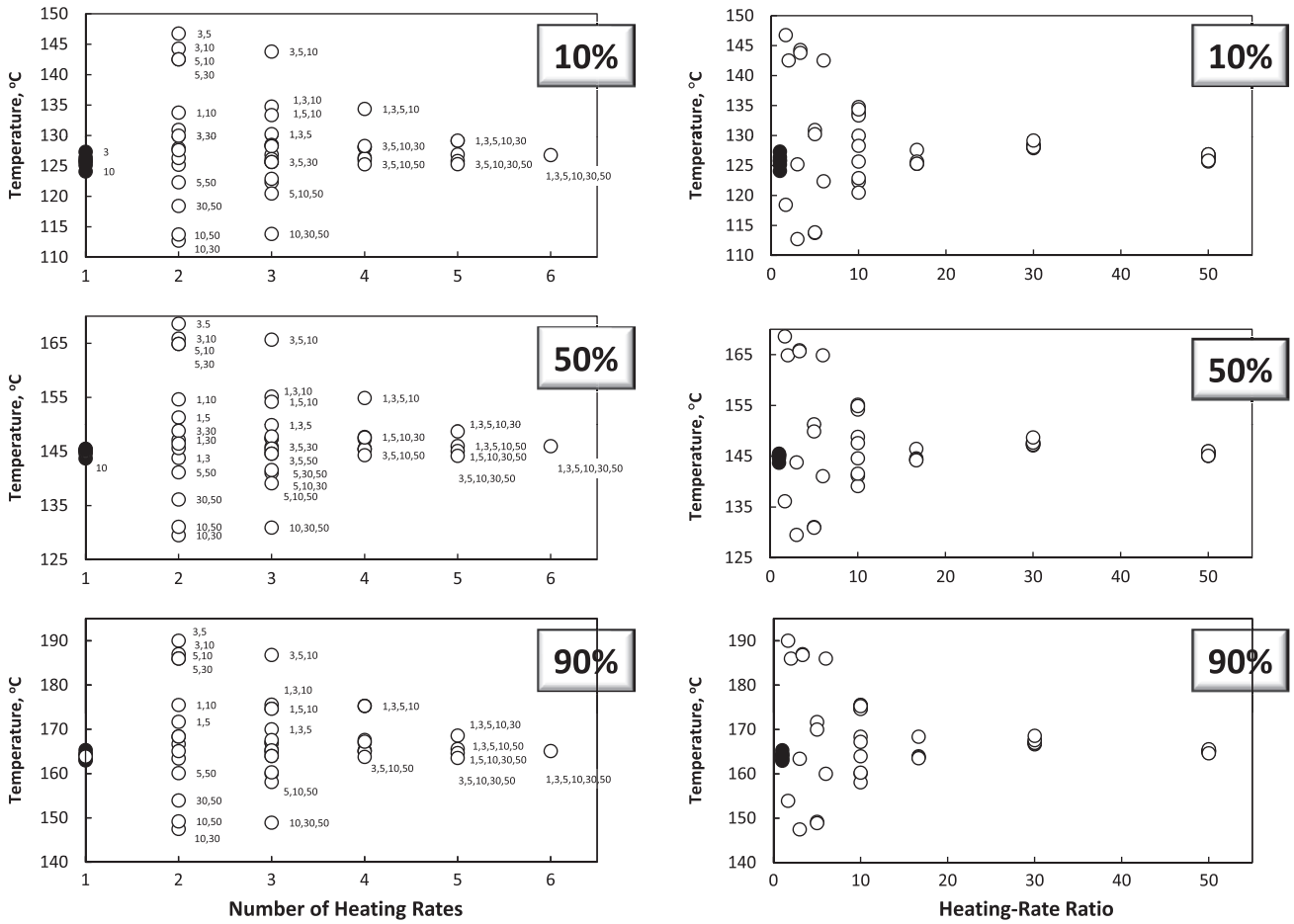

Figure 6. Calculated temperatures at 10%, 50%, and 90% transformation ratio (TR) based on assumed heating rate of 3°C/m.y. and kinetic parameters determined from various combinations of Pyromat II heating rates (1, 3, 5, 10, 30, and 50°C/min) for the Kimmeridge Clay sample (Table 3). Solid symbols are for single-ramp experiments with fixed frequency factor ($A = 1 \times 10^{14}$ sec^{-1}), and open symbols are for multiple-ramp experiments in which A was optimized. Selected symbols are labeled with the corresponding ramps (left). The heating-rate ratio (right) is the maximum divided by the minimum ramp rate.

Figures 6 and 7). This might be expected because the fixed and optimized A values are similar (1×10^{14} sec^{-1} and 1.28×10^{14} sec^{-1}, respectively; Table 3). However, the predicted TR temperatures for the Monterey Shale sample based on the six-ramp experiment are significantly lower than those for the single-ramp, fixed A method, because the fixed and optimized A values differ substantially (1×10^{14} sec^{-1} and 1.11×10^{13} sec^{-1}, respectively).

Six single-ramp pyrolysis experiments with fixed frequency factor (1×10^{14} sec^{-1}) for the Kimmeridge Clay sample at 1, 3, 5, 10, 30, and 50°C/min (number of ramps = 1; Figure 6, solid symbols at left) show narrow ranges of calculated temperature at TR of 10%, 50%, and 90% [124.1–127.3°C (3.2°C), 143.7–145.5°C (1.8°C), and 163.0–165.3°C (2.3°C), respectively; Table 4]. These single-ramp predictions of temperature correspond reasonably well with those based on a six-ramp experiment with an optimized frequency factor (number of ramps = 6; Figure 6) in which calculated temperatures at TR of 10%, 50%, and 90% are 126.8°, 146.0°, and 165.1°C, respectively. Therefore, if other ramps were not considered (e.g., two-, three-, four-, and five-ramp experiments), then one might conclude that the temperatures calculated from a single-ramp Kimmeridge Clay pyrolysis experiment at 10%, 50%, and 90% TR are as reliable as those based on a six-ramp experiment.

However, the data show that parameters from multiple-ramp experiments are generally more precise than those based on fewer ramps. The scatter in

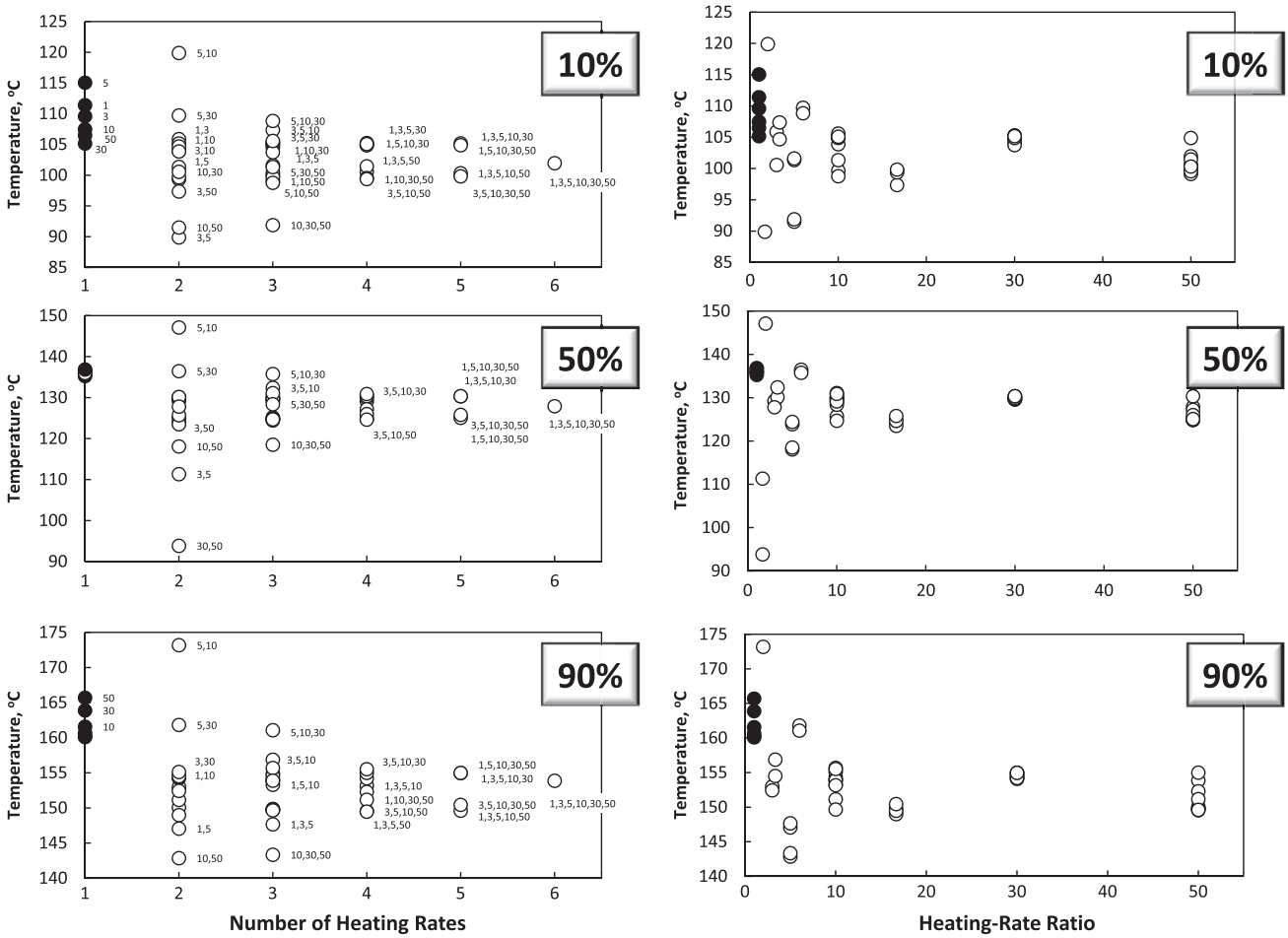

Figure 7. Calculated temperatures at 10%, 50%, and 90% transformation ratio (TR) based on assumed heating rate of 3°C/m.y. and kinetic parameters determined from various combinations of Pyromat II heating rates (1, 3, 5, 10, 30, and 50°C/min) for the Monterey Shale sample (Table 3). Solid symbols are for single-ramp experiments with fixed frequency factor ($A = 1 \times 10^{14}$ sec^{-1}), and open symbols are for multiple-ramp experiments in which A was optimized. Selected symbols are labeled with the corresponding ramps (left). The heating-rate ratio (right) is the maximum divided by the minimum ramp rate.

predicted temperatures decreases from two- to six-ramp experiments (Figures 6, 7, left). For example, optimized temperatures at 10%, 50%, and 90% TR for the Kimmeridge Clay using combinations of two, three, four, five, and six ramps show wide scatter that decreases with increasing number of ramps. Two-ramp Kimmeridge Clay experiments (number of ramps = 2; Figure 6, left) include fifteen combinations of Pyromat II experiments (Table 3): 1,3°; 1,5°; 1,10°; 1,30°; 1,50°; 3,5°; 3,10°; 3,30°; 3,50°; 5,10°; 5,30°; 5,50°; 10,30°; 10,50°; and 30,50°C/min. The two-ramp experiments show a wide range of calculated temperatures at 10% TR (34.0°C; Table 3), which decrease from three- to four- to five- to six-ramp experiments (range = 30.0°C, 9.1°C, 3.9°C, and 0°C, respectively). This result suggests that the similar calculated temperatures for the single- and six-ramp Kimmeridge Clay experiments are fortuitous. One might assume that six-ramp runs yield the most reliable temperatures. However, as discussed below, more reliable temperature predictions at 10%, 50%, and 90% TR may be achieved by excluding the faster ramps (e.g., 50°C/min), particularly if too large a sample is used for pyrolysis.

Consistent with the above, the data for the Monterey Shale (Figure 7, left) indicate that more ramps result in more precise determinations of temperature at 10%, 50%, and 90% TR. However, the

Table 4. Ranges and Average Temperatures Calculated Using Kinetics05 at 10%, 50%, and 90% Transformation Ratio for Kimmeridge Clay and Monterey Shale Whole-Rock Samples Pyrolyzed at Various Heating Rates Using Pyromat II*

			Range (°C)			Average (°C)		
Sample	Number of Heating Ramps	Number of Experiments	10% TR	50% TR	90% TR	10% TR	50% TR	90% TR
Kimmeridge Clay	1 (Fixed *A*)	6	3.21	1.78	2.34	125.77	144.90	164.03
	2	15	34.03	39.09	42.53	129.66	149.33	169.26
	3	16	29.95	34.75	37.90	127.30	146.62	166.20
	4	8	9.09	10.57	11.51	127.82	147.27	167.03
	5	4	3.87	4.50	5.05	126.79	146.00	165.58
	6	1	0	0	0	126.79	145.98	165.08
Monterey Shale	1 (Fixed *A*)	6	9.89	1.60	5.60	109.20	136.11	162.02
	2	15	49.62	53.29	56.08	100.21	125.45	149.95
	3	16	16.95	17.26	17.72	102.39	127.71	152.38
	4	8	5.87	6.24	6.05	102.64	127.88	152.55
	5	4	5.35	5.28	5.38	102.55	127.89	152.51
	6	1	0	0	0	101.96	127.90	153.87

*The single-ramp results consist of six pyrolysis experiments at 1, 3, 5, 10, 30, and 50°C/min using a constant frequency factor ($A = 1 \times 10^{14}$ sec^{-1}), as recommended by Waples et al. (2002, 2010). The two- through six-ramp results consist of all combinations of the six heating rates using an optimized *A*. Temperatures at 10%, 50%, and 90% transformation ratio (TR) were calculated assuming a geologic heating rate of 3°C/m.y.

temperatures calculated for single-ramp Monterey Shale experiments with fixed *A* (1×10^{14} sec^{-1}; solid symbols in Figure 7) are unlike those for the six-ramp experiment with optimized *A*. This result shows that single-run kinetic parameters are not reliable for all samples. Six single-ramp experiments on aliquots of the Monterey Shale sample at 1, 3, 5, 10, 30, and 50°C/min (number of ramps = 1; Figure 7, left) show various ranges of calculated temperature at 10%, 50%, and 90% TR (105.2–115.0°C [9.8°C], 135.3–136.9°C [1.6°C], and 160.1–165.7°C [5.6°C], respectively; Table 4). These single-ramp predictions of temperature differ from those based on six ramps (number of ramps = 6; Figure 7, left) where calculated temperatures at 10%, 50%, and 90% TR are 102.0°, 127.9°, and 153.9°C, respectively. As with the Kimmeridge Clay results, the Monterey Shale data clearly show that more ramps result in more precise calculated temperatures at 10%, 50%, and 90% TR.

Precision of the temperature predictions increases with a wider range of ramps, as measured by the ratio of the maximum to minimum ramps (R_r, Figures 6, 7, right). Temperature predictions using lower R_r generally yield more variable results. Single-ramp experiments with fixed *A* have R_r of 1. The highest R_r of 50 (R_{r50} = 50/1°C/min) includes 10 different combinations of heating rates that were each used to calculate temperatures at 10%, 50%, and 90% TR. These experiments include the six-ramp (1, 3, 5, 10, 30, and 50°C), five-ramp, four-ramp, three-ramp, and two-ramp runs (Table 4). The R_{r50} experiments for Kimmeridge Clay predict temperatures near 126.3, 145.6, and 165.1°C at 10%, 50%, and 90% TR, respectively, with standard deviations <0.5°C (Table 4). One- or two-ramp experiments can yield calculated temperatures that are fortuitously similar to those from five- or six-ramp experiments, but the results are not generally reliable, as demonstrated by the Monterey Shale data and Figure 3.

When combinations of pyrolysis heating rates are used in the discrete activation energy method, the 50°C/min rate contributes to significantly lower calculated temperatures and higher standard deviations at 10%, 50%, and 90% TR compared to combinations of lower heating rates (Figures 6, 7, left). For example, many of the labels indicating pyrolysis heating-rate combinations that include 50°C/min in

Figures 6 and 7 (left) occur in the lower temperature portion of each figure at 10%, 50%, and 90% TR. These comparisons of temperature at different TR assume a 3°C/m.y. geological heating rate. Furthermore, the $R_{r16.7}$ experiments for Kimmeridge Clay in Table 4 omit the 1°C ramp and show higher standard deviations for the calculated temperature at 10%, 50%, and 90% TR (1.1%, 1.1%, and 2.3%, respectively), whereas the R_{r30} experiments omit the 50°C ramp and show lower standard deviations (0.4%, 0.5%, 0.6%, respectively). Similar observations apply to the Monterey Shale experiments. $R_{r16.7}$ experiments for the Monterey Shale show higher standard deviations for calculated temperature at 10%, 50%, and 90% TR (1.0%, 0.8%, and 0.5%, respectively), whereas the ramp R_{r30} experiments show lower values (0.6%, 0.3%, and 0.3%, respectively).

However, fast ramps such as 50°C/min should be used with caution. The 50°C/min ramp (0.833°C/s) may be too fast to allow temperature equilibration throughout the sample, and therefore the thermocouple temperature at any time may be lower than that in the rock. The data in Table 4 support this interpretation. For example, the R_{r30} experiments for Kimmeridge Clay omit the 50°C ramp and show higher calculated temperatures at 10%, 50%, and 90% TR (128.3, 147.6, and 167.3°, respectively), whereas the $R_{r16.7}$ experiments omit the 1°C ramp, retain the 50°C ramp, and show lower calculated temperatures (126.0, 144.9, 164.9°C, respectively). Similar observations apply to the Monterey Shale experiments. The R_{r30} experiments for Monterey Shale show higher calculated temperatures at 10%, 50%, and 90% TR (104.7, 130.0, and 154.6, respectively), whereas the $R_{r16.7}$ experiments omit the 1°C ramp, retain the 50°C ramp, and show lower calculated temperatures (99.1, 124.7, 149.7°C, respectively).

Sample Size and Heating Rate

The accuracy of temperature measurements partly depends on proximity of the thermocouple to the sample, the thermal gradient across the sample region, and the relative size of the sample and thermocouple. Achieving maximum accuracy requires intimate contact between the thermocouple and sample and minimal mass for both. A transient heating effect may explain the data for fast- versus slow-ramp experiments in Figures 6 and 7 (left). Slow rate experiments (e.g., 1, 3, 10°C/min; 5, 10°C/min; or 3, 5, 10°C/min) typically predict higher temperatures than the six-ramp experiment in Figures 6 and 7, whereas faster rate experiments (e.g., 30, 50°C/min or 10, 30, 50°C/min) predict lower temperatures. Both slow and fast pyrolysis heating rates have been criticized. As discussed below, fast versus slow ramps are subject to error due to limited heat transfer or changes in product volatility, respectively.

Differences between the furnace and sample temperature are more severe with greater sample mass and faster heating rate (Vyazovkin et al., 2011). For example, Burnham et al. (1987) showed that a 50°C/min pyrolysis ramp yields a 2.2°C difference between the Rock-Eval thermocouple and the source rock in the sample holder, which they attributed to delay in heat transfer between the carrier gas and the sample. Reducing the heat demand of the sample would reduce that difference, as would the use of helium (e.g., Pyromat II), which has better thermal conductivity than the diatomic nitrogen used in the Rock-Eval instrument.

Based on thermogravimetry of typical polymers, Lyon et al. (2012, their figure 9) derived a quantitative relationship between heating rate and sample mass for an error of 5% in the measured maximum reaction rate. From this relationship, <5% error in the maximum reaction rate is expected for 3- and 10-mg samples at heating rates less than 20°C/min and 10°C/min, respectively. Our samples ranged from 3 to 10 mg, suggesting that heating rates up to about 20°C/min should yield reasonable data, but higher rates (e.g., 50°C/min) may be unreliable because of thermal lag. From this analysis, we recommend that the product of heating rate and sample size not exceed ~100 mg°C/min. Thus, reducing sample size for the 50°C/min experiments to 2 mg may have given more reliable results. Replicate analyses are recommended to compensate for potential heterogeneity in small samples.

Consistent with our observations, Schenk and Dieckmann (2004) used T_{max}-shift models

to show that lower ramps (0.1, 0.7, and 5°C/min) yield higher activation energies and frequency factors than do faster ramp experiments (5, 15, and 25°C). They concluded that slow heating rates provide the most reliable results. GeoForschungsZentrum in Potsdam uses 0.7, 2, and 5°C/min rate experiments (B. Horsfield, 2013, personal communication).

Oil yields from open-system pyrolysis experiments at atmospheric pressure decrease with lower heating rates (Campbell et al., 1978), apparently due to cross-linking related to longer liquid phase residence time. The delay between generation and volatilization increases with pressure (Burnham and Singleton, 1983). Burnham and Braun (1989) showed that the temperature and heating rate dependence of product volatility changes the apparent activation energy.

On the other hand, Burnham and Braun (1989) showed that product volatility changes as a function of heating rate, thus affecting detection temperature and apparent activation energy. The observed effect of lower pyrolysis heating rate on kinetic parameters was large for unswept oil evolution at 0.033 and 2°C/min, where Burnham (1991) found frequency factors 10–1000 times higher and activation energies 3–12 kcal/mol higher than those derived from equivalent samples at 1 to 50°C/min using Pyromat II. Despite these differences, the measured oil generation temperatures agreed fairly well with those predicted by Pyromat II. This shows that the compensation law can mask differences in kinetic parameters unless the extrapolation range is large.

Although it is tempting to presume that lower heating-rate experiments (e.g., <1°C/min) give more reliable extrapolations, product volatility may cause problems with the slower heating-rate experiments. Lower oil vapor pressures at lower heating rates require a greater extent of cracking for the product to be vaporized, which may also affect the apparent activation energy (Burnham and Singleton, 1983; Burnham and Braun, 1989).

At faster heating rates, the temperature recorded by the thermocouple may be lower than the average sample temperature due to limited thermal conductivity of the sample if the thermocouple is in the middle of the sample. As a result, fast pyrolysis heating-rate experiments, such as 50°C/min, may yield predicted temperatures at 10%, 50%, and 90% TR that are biased to low values (Figures 6, 7, left).

Higher laboratory heating rates appear to affect pyrolyzate yield. Peters et al. (2006b) concluded that calculations based on Rock-Eval pyrolysis overestimate expulsion factors and petroleum charge because low pressure and rapid removal of thermally cracked products by the carrier gas retard cross-linking and pyrobitumen formation that is otherwise favored by natural burial maturation. Expulsion factors and petroleum charge based on hydrous pyrolysis may also be high compared to nature for a similar reason (Lewan and Ruble, 2002). Lewan (1998) argues that because open-system pyrolysis experiments are 12 orders of magnitude faster than normal burial heating rates (~25°C/min versus $\sim 5 \times 10^{-12}$°C/min), little or no oil can be generated by this mechanism when extrapolated to geological heating rates (1–10°C/m.y.). However, semi-open experiments at elevated pressure that limit the generation of molecular hydrogen and in situ hydrogenation counteract that trend (Burnham and Singleton, 1983; Le Doan et al., 2013) and give yields and oil quality similar to hydrous pyrolysis.

Pyrolysis-based models, such as those described here, assume that the kinetics of petroleum generation from organic matter represent the rate-limiting step in expulsion. Others argue that retention and transport during primary migration represent the rate-limiting step (e.g., Stainforth, 2009). Most software that employs pyrolysis-based kinetics also includes saturation (e.g., Braun and Burnham, 1992) or absorption thresholds (e.g., Kelemen et al., 2006) that must be exceeded prior to expulsion. This paper does not address these issues. However, regardless of the method used to address kinetics, saturation, or adsorption, the thermal predictions from petroleum system modeling software are generally calibrated using corrected temperatures (e.g., Peters and Nelson, 2012) and other thermal indicators (e.g., Hantschel and Kauerauf, 2009) measured in wells from each study area. Thus, even if the kinetic results are not entirely accurate, model calibration can be used to yield reasonable temperature and maturity predictions. However, error in such kinetic results will propagate during calibration to one or more of the other output parameters.

Nucleation-Growth Modeling for Samples Having Narrow E_a Distributions

Kerogens with reaction profiles narrower than first-order reactions can introduce another type of error that can only be avoided by use of a nucleation-growth kinetic model (Burnham et al., 1996). For a single heating rate with optimized frequency factor, both the calculated E_a and A are larger than true values, as commonly observed for linear polymers. As the ramp range increases, the first-order frequency factor and activation energy approach true values, as estimated by the method of Kissinger (1957), because the shift in T_{max} with heating rate becomes more important relative to fitting the profile width. Typical ramp ranges for Pyromat II or similar systems tend to overestimate E_a, A, and the natural petroleum-generation temperature.

Seven samples from the 52-sample suite had reaction profiles narrower (typically by 10%) than the first-order activation energy derived by Kissinger's method (Table 5). These samples were re-analyzed by the nucleation-growth model in Kinetics05. The nucleation-growth model has the appropriate form for fitting some types of free-radical chain reactions. Table 6 compares the predicted petroleum generation temperatures for these samples with those obtained by discrete reactivity and Waples modeling. The table also includes results for three samples analyzed previously by Burnham et al. (1996). Table 6 shows that both the discrete and Waples methods have significant differences, comparable to those discussed in the previous section.

A Note on Compositional Kinetics

Compositional kinetics is used by many researchers to supplement the type of programmed pyrolysis kinetics described in this paper (e.g., Hantschel and Kauerauf, 2009), so a few key references are included here. Oil–gas kinetics (e.g., Pepper and Corvi, 1995) is the simplest form of compositional kinetics, in which gaseous hydrocarbons (C_1–C_5) are lumped together and oil consists of all heavier components (C_{6+}). Most compositional kinetic models include more than two components. Examples of these models include a four-component approach based on boiling-point classes (e.g., Behar et al., 1997); a 14-component scheme, which is particularly useful for predicting phase properties, such as gas-to-oil ratio (GOR; di Primio and Horsfield, 2006); and models of varying complexity involving species distinguished by molecular weight and chemical type (e.g., Braun and Burnham, 1992; Sweeney et al., 1995; Behar et al., 2008). The 14-component approach is based on combined open- and closed-system pyrolysis and accounts for the following classes: C_1, C_2, C_3, iC_4, nC_4, iC_5, nC_5, nC_6, C_7–C_{15}, C_{16}–C_{25}, C_{26}–C_{35}, C_{36}–C_{45}, C_{46}–C_{55}, and C_{55+}. Modeling results based on these data can

Table 5. Seven Selected Samples from Table 1 Having Narrow E_a Distributions by the Discrete Activation Energy Distribution Method Were Re-analyzed Using the Nucleation-Growth Method*

Sample	E_a Single–Multi (kcal/mol)	Log A Single–Multi	Temp. at 50% TR (°C), Free A	Temp. at 50% TR (°C), Single	Δ°C at 50% TR Discrete–Single	Kerogen Type**
1	4.81	1.57	131.0	147.6	−16.6	I
3	−0.63	0.06	152.3	153.5	−1.2	I
18	0.62	0.06	153.0	153.6	−0.6	I
25	3.82	1.23	140.9	153.6	−12.7	II
35	−2.16	−0.66	149.8	155.3	−5.5	I
36	0.10	−0.18	156.0	156.3	−0.3	I
49	4.37	0.98	140.2	152.1	−11.9	II

*Single = single-ramp pyrolysis experiment at 30°C/min using fixed frequency factor, $A = 1 \times 10^{14}$ sec^{-1}; Multi = simultaneous fit of all combinations of multiple ramp pyrolysis experiments (1°/min, 1°/min, 3°/min, 5°/min, 10°/min, 30°/min, and 50°/min) using free (optimized) A (sec^{-1}). Temperatures at 10%, 50%, and 90% transformation ratio (TR) were calculated assuming a geologic heating rate of 3°C/m.y.

**See the footnote for Table 1 and Peters and Cassa (1994).

Table 6. Comparison of Errors from Single-Ramp, Fixed Frequency Factor ($A = 1 \times 10^{14}$ sec^{-1}) and Multiple-Ramp (Optimized A) Pyrolysis Experiments Calculated Using the Discrete and Nucleation-Growth Models*

					Single Run, $A = 1 \times 10^{14}$ sec^{-1}		
Model	Sample	E_a (kcal/mol)	A (sec^{-1})	Temp. at 50% TR (°C)	E_a (kcal/mol)	Temp. at 50% TR (°C)	Δ°C at 50% TR Discrete–Single
Discrete	1	49.8	5.89×10^{12}	134.8	53.6	147.5	−12.7
	3	56.1	2.52×10^{14}	158.2	54.7	153.5	4.7
	18	58.0	9.71×10^{14}	164.4	54.4	153.6	10.8
	25	52.6	2.87×10^{13}	148.5	54.1	153.6	−5.1
	35	57.0	4.52×10^{14}	155.3	54.9	161.8	−6.5
	36	58.0	8.67×10^{14}	156.3	55.0	165.1	−8.8
	49	54.4	7.36×10^{13}	152.0	54.5	152.1	−0.1
	Broth	60.1	3.95×10^{15}	170.8	54.7	153.8	17.0
	GGU24	59.3	2.90×10^{15}	167.1	54.4	151.8	15.3
	Frejus	60.6	1.22×10^{16}	173.6	54.9	155.9	17.7
Nucleation Growth	1	48.7	2.72×10^{12}	131.1	53.6	147.5	−16.4
	3	54.1	7.98×10^{13}	152.3	54.7	153.5	−1.2
	18	54.2	8.69×10^{13}	153.0	54.4	153.6	−0.6
	25	50.6	5.83×10^{12}	140.9	54.1	153.6	−12.7
	35	53.0	4.44×10^{13}	149.8	54.9	161.8	−12.0
	36	54.9	1.52×10^{14}	156.0	55.0	165.1	−9.1
	49	50.5	1.05×10^{13}	140.2	54.5	152.1	−11.9
	Broth	55.6	2.59×10^{14}	157.5	54.7	153.8	3.7
	GGU24	56.0	5.38×10^{14}	158.2	54.4	151.8	6.4
	Frejus	57.4	7.27×10^{14}	164.8	54.9	155.9	8.9

*The nucleation-growth model is the preferred method for samples having narrow E_a distributions. The Broth, GGU24, and Frejus samples are from a previous study (Burnham et al., 1996). Temperatures at 10%, 50%, and 90% transformation ratio (TR) were calculated assuming a geologic heating rate of 3°C/m.y.

be expressed in pressure–volume–temperature phase diagrams and plots of generated components, GOR, and API gravity with increasing thermal maturity.

CONCLUSIONS

One-run, open-system pyrolysis experiments using a single heating ramp and fixed frequency factor to determine the petroleum generation kinetics for source-rock samples are appealing because they are faster and less expensive than multiple-ramp experiments. However, our results show that one-ramp pyrolysis experiments can yield kinetic results that are inconsistent with those from multiple-ramp experiments based on classic discrete activation energy distribution modeling (Table 1). Assuming a universal value for the frequency factor (e.g., 1×10^{14} or 2×10^{14} sec^{-1}) places undue reliance on temperature measurements that may not have sufficient accuracy to allow reliable kinetic determinations. The frequency factors for our samples show statistically significant differences. For a 52-sample dataset, frequency factors vary over four orders of magnitude ($\sim 10^{12}$–10^{16} sec^{-1}) and are reproducible within experimental precision. Burnham (1994) saw a similar range in frequency factors for his samples. Using his 1-2-3 rule, he calculated that adoption of a fixed frequency factor of 1×10^{14} sec^{-1} could result in an error as large as 20°C for geologic extrapolations.

For kerogens having narrow activation energy distributions, both single- and multiple-ramp discrete activation energy distribution models are unreliable and nucleation-growth models are necessary.

Our data show that the precision of kinetic results, as measured by calculated temperatures at 10%, 50%, and 90% TR, increases with the number of pyrolysis heating ramps in the range 1–50°C/min. Temperature ramps of 30 and 50°C/min may be too fast to obtain a good kinetic fit because of delayed heat transfer between the sample and thermocouple, although that effect can be mitigated by using smaller sample sizes. The product of heating rate and sample size should not exceed ~100 mg °C/min. A 20- to 30-fold variation in heating rate appears to be sufficient to derive good kinetics. We recommend at least three pyrolysis ramps, such as 1, 5, and 25°C/min or 1, 3, 9, and 27°C/min, and replicates at the extreme heating rates are important. Lower heating rates can be added if the rock is sufficiently organic rich to yield an acceptable signal or if kerogen isolates are prepared. Finally, whether these discrete kinetic models based on open-system pyrolysis are mechanistically appropriate for use in basin simulators remains debatable.

APPENDIX: EFFECT OF TEMPERATURE ERRORS ON KINETIC PARAMETERS AND GEOLOGIC EXTRAPOLATION

The Precision of Experimental Data section discussed three types of temperature error in the laboratory that influence kinetic parameters and proper extrapolation to geological time and temperature: (1) constant shift in measured temperatures, (2) temperature error that varies systematically with heating rate, and (3) random error. Error types 1 and 2 were demonstrated by Burnham et al. (1987). This appendix explores the effect of random error as discussed by Burnham (2014). Our intent is to explain the reason for the reduced variation in kinetic parameters as a function of heating-rate ratio (e.g., Figure 4) in view of the statistical variability of a single measurement on the Bellagio Road sample. Although not evident in Figure 4, errors associated with the highest and lowest heating rates have the greatest effect on calculated kinetic parameters.

A parametric study was performed using the Kissinger (1957) method, also known as the T_{max}-shift method, to demonstrate the effect of a single 2°C temperature error depending on whether it occurs in one of the extreme or in one of the intermediate heating rates (see also Burnham, 2014). An E_a of 54.00 kcal/mole and A of 1.00×10^{14} sec^{-1} were used for the reference kinetic parameters. As expected, all of the results from this study of random error follow a compensation law plot (Figure 8).

For three heating rates, one erroneous point in the logarithmic middle of the heating rate range has little effect on kinetic parameters (Table 7). For reference, three heating rates (1, 4, and 16°C/min) were selected for a calculated E_a of 54.00 kcal/mole and A of 1.00×10^{14} sec^{-1}. If a 2°C error in E_a is assumed for the middle heating rate (4°C/min), then the calculated error for E_a is only ~0.1 kcal/mol (53.90 versus 54.00 kcal/mole), A is slightly lower (9.53×10^{13} versus 1.00×10^{14} sec^{-1}), and the extrapolated error at 3°C/m.y. to geologic conditions is only 0.7°C (150.1 versus 150.8°C). However, if the same 2°C error occurred at one of the extreme heating rates (i.e., 16°C/min), the calculated E_a, A, and generation temperature under geologic conditions at 3°C/m.y. (51.93 kcal/mole, 2.18×10^{13} sec^{-1}, and 144.4°C) differ substantially from the reference results (54.00 kcal/mole, 1.00×10^{14} sec^{-1}, and 150.8°C, respectively).

At four heating rates, error in one of the two middle points has a greater effect, but error in the geologic extrapolation at 3°C/m.y. is only 1.6°C. However, the same 2°C error at one of the extreme heating rates results in an error of ≥2 kcal/mol and a geologic extrapolation error of ~6°C. The error is only slightly lower for four rather than three heating rates. Therefore, temperature errors for the highest or lowest heating rate experiments have the greatest impact on the kinetic results, and replicate analyses at these extreme rates are recommended.

Interestingly, the square of the correlation coefficient (r^2) does not indicate the accuracy of the geological prediction. The r^2 values near 1.0 reflect a better linear fit, but a good linear relationship does not assure that the line is the correct line. Errors in the middle heating rate range significantly influence r^2 but have little effect on the slope of the line, so error in geological extrapolations can still be large despite better r^2 values.

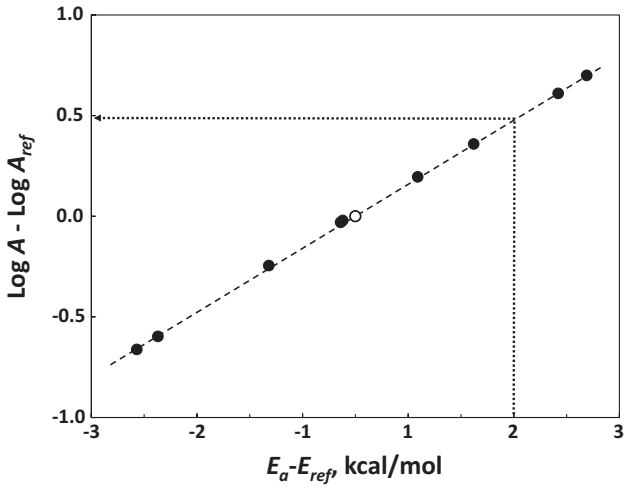

Figure 8. A compensation law plot (Table 7) shows a spread in activation energy (E_a) relative to a reference value (E_{ref}, open symbol) of approximately ±2 kcal/mol for a randomly located 2°C error at various heating rates spanning a decade range (1–10°C/min). The corresponding range in frequency factor (A) is roughly a factor of 4, and the error in extrapolation to geological heating rates, assuming 3°C/m.y., spans a range of about ±6°C. The dotted line shows an example in which an E_a error of 2 kcal/mol corresponds to slightly less than a four-fold increase in A; that is, $\log(4) = 0.6$.

Table 7. Kinetic Parameters Derived from Data Having a Single 2°C Error for One Data Point (Burnham, 2014)*

Test Paradigm	Heating Rates (°C/min)	Lab T_{max} (°C)	A (sec^{-1})	E_a (kcal/mol)	Correlation Coefficient, r^2	Geo T_{max}(°C)
Three heating rates	1	420.07	1.00×10^{14}	54.00	1.000	150.8
	4	444.18				
	16	469.99				
	1	420.07				
	4	**442.18**	9.53×10^{13}	53.88	0.998	150.1
	16	469.99				
	1	420.07				
	4	444.18				
	16	**467.99**	5.01×10^{14}	56.19	0.999	157.2
	1	420.07				
	4	444.18				
	16	**471.99**	2.18×10^{13}	51.93	0.999	144.4
Three heating rates + replicate	1	420.07				
	4	444.18				
	4	**442.18**	9.33×10^{13}	53.86	0.997	154.1
	16	469.99				
	1	420.07				
	4	444.18				
	16	**467.99**	2.29×10^{14}	55.12	0.999	150.1
	16	469.99				
Four heating rates	1	420.07	1.00×10^{14}	54.00	1.000	150.8
	2.5	435.82				
	6.5	453.02				
	16	469.99				
	1	420.07				
	2.5	**433.82**	5.69×10^{13}	53.18	0.998	148.0
	6.5	453.02				
	16	469.99				
	1	420.07				
	2.5	435.82				
	6.5	**451.02**	1.57×10^{14}	54.59	0.998	152.4
	16	469.99				
	1	420.07				
	2.5	435.82				
	6.5	453.02				
	16	**467.99**	4.08×10^{14}	55.92	0.999	156.5
	1	420.07				
	2.5	435.82				
	6.5	453.02				
	16	**471.99**	2.53×10^{13}	52.13	0.999	145.0

*A reference case with no error is given for both the three- and four-heating rate examples. Each rate experiment in which the 2°C error was applied is highlighted in bold. For all but the last example, the 2°C shift was to lower temperature, but approximately symmetrical results can be obtained for a 2°C shift to higher temperature.

REFERENCES CITED

Barth, T., B. J. Smith, and S. B. Nielsen, 1996, Do kinetic parameters from open pyrolysis describe petroleum generation by simulated maturation?: Bulletin of Canadian Petroleum Geology, v. 44, p. 446–457.

Behar, F., S. Kressman, J. L. Rudkiewicz, and M. Vandenbroucke, 1992, Experimental simulation in a confined system and kinetic modeling of kerogen and oil cracking: Organic Geochemistry, v. 19, p. 173–189, doi:10.1016/0146-6380(92)90035-V.

Behar, F., F. Lorant, and L. Mazeas, 2008, Elaboration of a new compositional kinetic schema for oil cracking: Organic Geochemistry, v. 39, p. 764–782, doi:10.1016/j.orggeochem.2008.03.007.

Behar, F., M. Vandenbroucke, Y. Tang, F. Marquis, and J. Espitalié, 1997, Thermal cracking of kerogen in open and closed systems: Organic Geochemistry, v. 26, p. 321–339, doi:10.1016/S0146-6380(97)00014-4.

Braun, R. L., and A. K. Burnham, 1987, Analysis of chemical reaction kinetics using a distribution of activation energies

and simpler models: Energy and Fuels, v. 1, p. 153–161, doi:10.1021/ef00002a003.

Braun, R. L., and A. K. Burnham, 1992, PMOD: A flexible model of oil and gas generation, cracking, and expulsion: Organic Geochemistry, v. 19, p. 161–172, doi:10.1016/0146-6380(92)90034-U.

Braun, R. L., A. K. Burnham, and J. G. Reynolds, 1991a, Oil and gas evolution kinetics for oil shale and petroleum source rocks determined from pyrolysis—TQMS data at multiple heating rates: Energy and Fuels, v. 6, p. 468–474, doi:10.1021/ef00034a017.

Braun, R. L., A. K. Burnham, J. G. Reynolds, and J. E. Clarkson, 1991b, Pyrolysis kinetics for lacustrine and marine source rocks by programmed pyrolysis: Energy and Fuels, v. 5, p. 192–204, doi:10.1021/ef00025a033.

Burnham, A. K., 1991, Oil evolution from a self-purging reactor: Kinetics and composition at 2°C/min and 2°C/h: Energy and Fuels, v. 5, p. 205–214, doi:10.1021/ef00025a034.

Burnham, A. K., 1992, Are laboratory-derived maturation kinetics reliable?: AAPG Annual Meeting, Calgary, Alberta, Canada, June 22–25, 1992, AAPG Search and Discovery Article #91012, accessed December 10, 2014, http://www.searchanddiscovery.com/abstracts/html/1992/annual/abstracts/0014c.htm.

Burnham, A. K., 1994, Comments on "The effects of the mineral matrix on the determination of kinetic parameters using modified Rock-Eval pyrolysis" by H. Dembicki Jr., and the resulting comment by R. Pelet: Organic Geochemistry, v. 21, p. 985–986, doi:10.1016/0146-6380(94)90058-2.

Burnham, A. K., 2014, Obtaining reliable phenomenological chemical kinetic models for real-world applications: Thermochimica Acta, v. 597, p. 35–40, doi:10.1016/j.tca.2014.10.006.

Burnham, A. K., and R. L. Braun, 1989, Development of a detailed model of petroleum formation, destruction, and expulsion from lacustrine and marine source rocks: Organic Geochemistry, v. 16, p. 27–39, doi:10.1016/0146-6380(90)90023-S.

Burnham, A. K., and R. L. Braun, 1999, Global kinetic analysis of complex materials: Energy and Fuels, v. 13, p. 1–22, doi:10.1021/ef9800765.

Burnham, A. K., R. L. Braun, T. T. Coburn, E. I. Sandvik, D. J. Curry, B. J. Schmidt, and R. A. Noble, 1996, An appropriate kinetic model for well-preserved algal kerogens: Energy and Fuels, v. 10, p. 49–59, doi:10.1021/ef950142s.

Burnham, A. K., R. L. Braun, H. R. Gregg, and A. M. Samoun, 1987, Comparison of methods for measuring kerogen pyrolysis rates and fitting kinetic parameters: Energy and Fuels, v. 1, p. 452–458, doi:10.1021/ef00006a001.

Burnham, A. K., B. J. Schmidt, and R. L. Braun, 1995, A test of the parallel reaction model using kinetic measurements on hydrous pyrolysis residues: Organic Geochemistry, v. 23, p. 931–939, doi:10.1016/0146-6380(95)00069-0.

Burnham, A. K., and M. F. Singleton, 1983, High pressure pyrolysis of Green River oil shale. Geochemistry and chemistry of oil shale, *in* F. P. Miknis and J. F. McKay, eds., ACS Symposium Series 230: Washington, D.C., American Chemical Society, p. 335–351.

Campbell, J. H., G. J. Koskinas, N. D. Stout, and T. T. Coburn, 1978, Oil shale retorting: Effects of particle size and heating rate on oil evolution and intraparticle oil degradation: In Situ, v. 2, p. 1–47.

Clementz, D. M., 1979, Effect of oil and bitumen saturation on source-rock pyrolysis: AAPG Bulletin, v. 63, p. 2227–2232.

Cordes, H. F., 1968, The preexponential factors for solid-state thermal decomposition: The Journal of Physical Chemistry, v. 72, p. 2185–2189, doi:10.1021/j100852a052.

di Primio, R., and B. Horsfield, 2006, From petroleum-type organofacies to hydrocarbon phase prediction: AAPG Bulletin, v. 90, p. 1031–1058, doi:10.1306/02140605129.

Dieckmann, V., 2005, Modelling petroleum formation from heterogeneous source rocks: The influence of frequency factors on activation energy distribution and geological prediction: Marine and Petroleum Geology, v. 22, p. 375–390, doi:10.1016/j.marpetgeo.2004.11.002.

Dieckmann, V., B. Horsfield, and H. J. Schenk, 2000, Heating rate dependency of petroleum-forming reactions: Implications for compositional kinetic predictions: Organic Geochemistry, v. 31, p. 1333–1348, doi:10.1016/S0146-6380(00)00105-4.

Espitalié, J., 1986, Use of T_{max} as a maturation index for different types of organic matter. Comparison with vitrinite reflectance: 1st IFP Exploration Research Conference, Carcans, France, June 3–7, 1985, *in* J. Burris, ed., Thermal modeling in sedimentary basins: Paris, Editions Technip, p. 475–496.

Espitalié, J., P. Ungerer, I. Irwin, and F. Marquis, 1988, Primary cracking of kerogens. Experimenting and modeling C_1, C_2–C_5, C_6–C_{15} and C_{15+} classes of hydrocarbons formed: Organic Geochemistry, v. 13, p. 893–899, doi:10.1016/0146-6380(88)90243-4.

Flynn, J. H., and R. E. Florin, 1985, Degradation and pyrolysis mechanisms, *in* S. A. Liebman and E. J. Levy, eds., Pyrolysis and GC in polymer analysis: New York, Marcel Dekker, p. 149–208.

Flynn, J. H., and L. A. Wall, 1966, A quick, direct method for the determination of activation energy from thermogravimetric data: Polymer Letters, v. 4, p. 323–328, doi:10.1002/pol.1966.110040504.

Hantschel, T., and A. I. Kauerauf, 2009, Fundamentals of basin and petroleum systems modeling: New York, Springer, 475 p.

Horsfield, B., U. Disko, and F. Leistner, 1989, The micro-scale simulation of maturation: Outline of a new technique and its potential applications: Geologische Rundschau, v. 78, p. 361–373, doi:10.1007/BF01988370.

Issler, D. R., and L. R. Snowdon, 1990, Hydrocarbon generation kinetics and thermal modeling, Beaufort-Mackenzie Basin: Bulletin of Canadian Petroleum Geology, v. 38, p. 1–16.

Jarvie, D. M., 1991, Factors affecting Rock-Eval derived kinetic parameters: Chemical Geology, v. 93, p. 79–99, doi:10.1016/0009-2541(91)90065-Y.

Jarvie, D. M., and L. L. Lundell, 2001, Kerogen type and thermal transformation of organic matter in the Miocene Monterey Formation, *in* C. M. Isaacs and J. Rullkötter, eds., The Monterey Formation: From rocks to molecules: New York, Columbia University Press, p. 269–295.

Kelemen, S. R., C. C. Walters, D. Ertas, and H. Freund, 2006, Petroleum expulsion Part 3: A model of chemically driven fractionation during expulsion of petroleum from kerogen: Energy and Fuels, v. 20, p. 309–319, doi:10.1021/ef058023s.

Kissin, Y. V., 1987, Catagenesis and composition of petroleum: Origin of n-alkanes and isoalkanes in petroleum crudes: Geochimica et Cosmochimica Acta, v. 51, p. 2445–2457, doi:10.1016/0016-7037(87)90296-1.

Kissinger, H. E., 1957, Reaction kinetics in differential thermal analysis: Analytical Chemistry, v. 29, p. 1702–1706, doi:10.1021/ac60131a045.

Kuhn, P. P., R. di Primio, R. Hill, J. R. Lawrence, and B. Horsfield, 2012, Three-dimensional modeling study of the low-permeability petroleum system of the Bakken Formation: AAPG Bulletin, v. 96, p. 1867–1897, doi:10.1306/03261211063.

Lakshmanan, C. C., M. L. Bennett, and N. White, 1991, Implications of multiplicity in kinetic parameters to petroleum exploration: Distributed activation energy models: Energy and Fuels, v. 5, p. 110–117, doi:10.1021/ef00025a019.

Le Doan, T. V., N. W. Bostrom, A. K. Burnham, R. L. Kleinberg, A. E. Pomerantz, and P. Allix, 2013, Green River oil shale pyrolysis: Semi-open conditions: Energy and Fuels, v. 27, p. 6447–6459, doi:10.1021/ef401162p.

Levenberg, K., 1944, A method for the solution of certain nonlinear problems in least squares: Quarterly of Applied Mathematics, v. 2, p. 164–168.

Lewan, M. D., 1998, Reply to the comment by A.K. Burnham on "Experiments on the role of water in petroleum formation": Geochimica et Cosmochimica Acta, v. 62, p. 2211–2216, doi:10.1016/S0016-7037(98)00150-1.

Lewan, M. D., and T. E. Ruble, 2002, Comparison of petroleum generation kinetics by isothermal hydrous and nonisothermal open-system pyrolysis: Organic Geochemistry, v. 33, p. 1457–1475, doi:10.1016/S0146-6380(02)00182-1.

Lewan, M. D., J. C. Winters, and J. H. McDonald, 1979, Generation of oil-like pyrolyzates from organic-rich shales: Science, v. 203, p. 897–899, doi:10.1126/science.203.4383.897.

Lyon, R. E., N. Safronava, J. Senese, and S. I. Stoliarov, 2012, Thermokinetic model of sample response in nonisothermal analysis: Thermochimica Acta, v. 545, p. 82–89, doi:10.1016/j.tca.2012.06.034.

Magoon, L. B., and W. G. Dow, 1994, The petroleum system, *in* L. B. Magoon and W. G. Dow, eds., The petroleum system—From source to trap: AAPG Memoir 60, p. 3–24.

Ozawa, T., 1965, A new method for analyzing thermogravimetric data: Bulletin of the Chemical Society of Japan, v. 38, p. 1881–1886, doi:10.1246/bcsj.38.1881.

Pepper, A. S., and P. J. Corvi, 1995, Simple kinetic models of petroleum formation: Part I—Oil and gas generation from kerogen: Marine and Petroleum Geology, v. 12, p. 291–319, doi:10.1016/0264-8172(95)98381-E.

Peters, K. E., 1986, Guidelines for evaluating petroleum source rock using programmed pyrolysis: AAPG Bulletin, v. 70, p. 318–329.

Peters, K. E., and M. R. Cassa, 1994, Applied source rock geochemistry, *in* L. B. Magoon and W. G. Dow, eds., The petroleum system—From source to trap: AAPG Memoir 60, p. 93–120.

Peters, K. E., D. J. Curry, and M. Kacewicz, 2012, An overview of basin and petroleum system modeling: Definitions and concepts, *in* K. E. Peters, D. Curry, and M. Kacewicz, eds., Basin modeling: New horizons in research and applications: AAPG Hedberg Series 4, p. 1–16.

Peters, K. E., T. Hantschel, A. I. Kauerauf, Y. Tang, and B. Wygrala, 2013, Recent advances in petroleum system modeling of geochemical processes: TSR, SARA, and biodegradation: AAPG Annual Meeting, Pittsburg, PA, AAPG Search and Discovery Article #41261, accessed December 10, 2014, http://www.searchanddiscovery.com/pdfz/documents/2013/41261peters/ndx_peters.pdf.html.

Peters, K. E., L. B. Magoon, K. J. Bird, Z. C. Valin, and M. A. Keller, 2006b, North Slope, Alaska: Source rock distribution, richness, thermal maturity, and petroleum charge: AAPG Bulletin, v. 90, p. 261–292, doi:10.1306/09210505095.

Peters, K. E., and P. H. Nelson, 2012, Criteria to determine borehole formation temperatures for calibration of basin models, *in* N. B. Harris and K. E. Peters, eds., Analyzing the thermal history of sedimentary basins: Methods and case studies: SEPM Special Publication 103, p. 5–15.

Peters, K. E., C. C. Walters, and P. J. Mankiewicz, 2006a, Evaluation of kinetic uncertainty in numerical models of petroleum generation: AAPG Bulletin, v. 90, p. 1–20, doi:10.1306/08090504134.

Reynolds, J. G., and A. K. Burnham, 1995, Comparison of kinetic analysis of source rocks and kerogen concentrates: Organic Geochemistry, v. 23, p, 11–19, doi:10.1016/0146-6380(94)00114-G.

Reynolds, J. G., A. K. Burnham, and T. O. Mitchell, 1995, Kinetic analysis of California petroleum source rocks by programmed temperature pyrolysis: Organic Geochemistry, v. 23, p. 109–120, doi:10.1016/0146-6380(94)00121-G.

Ritter, U., M. B. Myhr, T. Vinge, and K. Aareskjold, 1995, Experimental heating and kinetic models of source rocks: Comparison of different methods: Organic Geochemistry, v. 23, p. 1–9, doi:10.1016/0146-6380(94)00108-D.

Sanchez-Jimenez, P. E., L. A. Perez-Maqueda, A. Perejon, and J. M. Criado, 2010, A new model for the kinetic analysis of thermal degradation of polymers driven by random scission: Polymer Degradation and Stability, v. 95, p. 733–739, doi:10.1016/j.polymdegradstab.2010.02.017.

Schenk, H. J., and V. Dieckmann, 2004, Prediction of petroleum formation: The influence of laboratory heating rates on kinetic parameters and geological extrapolations: Marine and Petroleum Geology, v. 21, p. 79–95, doi:10.1016/j.marpetgeo.2003.11.004.

Schenk, H. J., and B. Horsfield, 1993, Kinetics of petroleum generation by programmed-temperature closed- versus open-system pyrolysis: Geochimica et Cosmochimica Acta, v. 57, p. 623–630, doi:10.1016/0016-7037(93)90373-5.

Schenk, H. J., and B. Horsfield, 1998, Using natural maturation series to evaluate the utility of parallel reaction kinetics models: An investigation of Toarcian shales and Carboniferous

coals, Germany: Organic Geochemistry, v. 29, p. 137–154, doi:10.1016/S0146-6380(98)00139-9.

Stainforth, J. G., 2009, Practical kinetic modeling of petroleum generation and expulsion: Marine and Petroleum Geology, v. 26, p. 552–572, doi:10.1016/j.marpetgeo.2009.01.006.

Sundararaman, P., P. H. Merz, and R. G. Mann, 1992, Determination of kerogen activation energy distribution: Energy and Fuels, v. 6, p. 793–803, doi:10.1021/ef00036a015.

Sweeney, J. J., R. L. Braun, A. K. Burnham, S. Talukdar, and C. Vallejos, 1995, Chemical kinetic model of hydrocarbon generation, expulsion, and destruction applied to the Maracaibo basin, Venezuela: AAPG Bulletin, v. 79, p. 1515–1532.

Sweeney, J. J., A. K. Burnham, and R. L. Braun, 1987, A model of hydrocarbon generation from type I kerogen: Application to Uinta Basin, Utah: AAPG Bulletin, v. 71, p. 967–985.

Tegelaar, E. W., and R. A. Noble, 1994, Kinetics of hydrocarbon generation as a function of the molecular structure of kerogen as revealed by pyrolysis-gas chromatography: Organic Geochemistry, v. 22, p. 543–574, doi:10.1016/0146-6380(94)90125-2.

Tissot, B. P., and J. Espitalié, 1975, L'evolution thermique de la matiere organique des sediments: applications d'une simulation mathematizue: Revue de l'Institut Français du Petrole, v. 30, p. 743–778, doi:10.2516/ogst:1975026.

Tissot, B. P., and D. H. Welte, 1984, Petroleum formation and occurrence: New York, Springer-Verlag, 699 p.

Ungerer, P., 1990, State of the art of research in kinetic modeling of oil formation and expulsion: Organic Geochemistry, v. 16, p. 1–25, doi:10.1016/0146-6380(90)90022-R.

Ungerer, P., and R. Pelet, 1987, Extrapolation of the kinetics of oil and gas formation from laboratory experiments to sedimentary basins: Nature, v. 327, p. 52–54, doi:10.1038/327052a0.

Vyazovkin, S., A. K. Burnham, J. M. Criado, L. A. Pérez-Maqueda, C. Popescu, and N. Sbirrazzuoli, 2011, ICTAC Kinetics Committee recommendations for performing kinetic computations on thermal analysis data: Thermochimica Acta, v. 520, p. 1–19, doi:10.1016/j.tca.2011.03.034.

Vyazovkin, S., K. Chrissafis, M. L. Di Lorenzo, N. Koga, M. Pijolet, B. Roduit, N. Sbirrazzuoli, and J. J. Sunol, 2014, ICTAC Kinetics Committee recommendations for collecting experimental thermal analysis data for kinetic computations: Thermochemica Acta, v. 590, p. 1–23, doi:10.1016/j.tca.2014.05.036.

Vyazovkin, S., and C. A. Wight, 1999, Model-free and model-fitting approaches to kinetic analysis of isothermal and nonisothermal data: Thermochimica Acta, v. 340–341, p. 53–68, doi:10.1016/S0040-6031(99)00253-1.

Walters, C. C., H. Freund, S. R. Keleman, P. Peczak, and D. J. Curry, 2007, Predicting oil and gas compositional yields via chemical structure-chemical yield modeling (CS-SYM): Part 2—Application under laboratory and geologic conditions: Organic Geochemistry, v. 38, p. 306–322, doi:10.1016/j.orggeochem.2006.09.010.

Waples, D. W., J. E. Leonard, R. Coskey, S. Safwat, and R. Nagdy, 2010, A new method for obtaining personalized kinetics from archived Rock-Eval data, applied to the Bakken Formation, Williston Basin (abs.): AAPG International Convention, Calgary, AAPG Search and Discovery Article #90108, accessed January 31, 2015, www.searchanddiscovery.com/pdfz/abstracts/pdf/2010/intl/abstracts/ndx_waples02.pdf.html.

Waples, D. W., and V. S. Nowaczewski, 2013, Source-rock kinetics, accessed February 6, 2015, https://siriusdummy.files.wordpress.com/2013/11/perspective-on-sr-kinetics-ss.pdf.

Waples, D. W., M. Suizu, and H. Kamata, 1992, The art of maturity modeling: Part 2—Alternative models and sensitivity analysis: AAPG Bulletin, v. 76, p. 47–66.

Waples, D. W., A. Vera, and J. Pacheco, 2002, A new method for kinetic analysis of source rocks: Development and application as a thermal and organic facies indicator in the Tithonian of the Gulf of Campeche, Mexico (abs.): 8th Latin American Congress on Organic Geochemistry, Cartagena, p. 296–298.

Welte, D. H., B. Horsfield, and D. R. Baker, eds., 1997, Petroleum and basin evolution: Berlin, Springer, 535 p.

Welte, D. H., and M. A. Yükler, 1981, Petroleum origin and accumulation in basin evolution—A quantitative model: AAPG Bulletin, v. 65, p. 1387–1396.